# Yin/Yang associated differential responses to *Psoralea corylifolia* Linn. In rat models: an integrated metabolomics and transcriptomics study

Ming-Liang Zhang[1†], Xu Zhao[2,3†], Wei-Xia Li[1,4], Xiao-Yan Wang[1,4], Ming Niu[2,3], Hui Zhang[1,4], Yu-Long Chen[4], De-Xin Kong[1,4], Yuan Gao[5], Yu-Ming Guo[2,3], Zhao-Fang Bai[2,3], Yan-Ling Zhao[6,7*], Jin-Fa Tang[1*] and Xiao-He Xiao[2*]

## Abstract

**Ethnopharmacological relevance**  *Psoralea corylifolia* Linn. (BGZ) is a commonly used traditional Chinese medicine (TCM) for the treatment of kidney-yang deficiency syndrome (Yang$_{syn}$) with good curative effect and security. However, BGZ was also reported to induce liver injury in recent years. According to TCM theory, taking BGZ may induce a series of adverse reactions in patients with kidney-yin deficiency syndrome (Yin$_{syn}$), which suggests that BGZ-induced liver damage may be related to its unreasonable clinical use.

**Aim of the study**  Liver injury caused by TCM is a rare but potentially serious adverse drug reaction, and the identification of predisposed individuals for drug-induced liver injury (DILI) remains challenging. The study aimed to investigate the differential responses to BGZ in Yang$_{syn}$ and Yin$_{syn}$ rat models and identify the corresponding characteristic biomarkers.

**Materials and methods**  The corresponding animal models of Yang$_{syn}$ and Yin$_{syn}$ were induced by hydrocortisone and thyroxine + reserpine respectively. Body weight, organ index, serum biochemistry, and Hematoxylin and Eosin (HE) staining were used to evaluate the liver toxicity effect of BGZ on rats with Yang$_{syn}$ and Yin$_{syn}$. Transcriptomics and metabonomics were used to screen the representative biomarkers (including metabolites and differentially expressed genes (DEGs)) changed by BGZ in Yang$_{syn}$ and Yin$_{syn}$ rats, respectively.

**Results**  The level changes of liver organ index, alanine aminotransferase (ALT), and aspartate aminotransferase (AST), suggested that BGZ has liver-protective and liver-damaging effects on Yang$_{syn}$ and Yin$_{syn}$ rats, respectively, and the results also were confirmed by the pathological changes of liver tissue. The results showed that 102 DEGs and 27 metabolites were significantly regulated related to BGZ's protective effect on Yang$_{syn}$, which is mainly

†Ming-Liang Zhang and Xu Zhao contributed equally to this work.

*Correspondence:
Yan-Ling Zhao
zhaoyl2855@126.com
Jin-Fa Tang
a0519@163.com
Xiao-He Xiao
pharmacy302xxh@126.com
Full list of author information is available at the end of the article

Zhang *et al. Chinese Medicine*    (2023) 18:102

Page 2 of 23

associated with the glycerophospholipid metabolism, arachidonic acid metabolism, pantothenate, and coenzyme A (CoA) biosynthesis pathways. While 28 DEGs and 31 metabolites, related to the pathway of pantothenate and CoA biosynthesis, were significantly regulated for the BGZ-induced liver injury in Yin$_{syn}$. Furthermore, 4 DEGs (aldehyde dehydrogenase 1 family member B1 (Aldh1b1), solute carrier family 25 member 25 (Slc25a25), Pim-3 proto-oncogene, serine/threonine kinase (Pim3), out at first homolog (Oaf)) and 4 metabolites (phosphatidate, phosphatidylcholine, N-Acetylleucine, biliverdin) in the Yang$_{syn}$ group and 1 DEG [galectin 5 (Lgals5)] and 1 metabolite (5-amino-1-(5-phospho-D-ribosyl)imidazole-4-carboxylate) in Yin$_{syn}$ group were significantly correlated to the ALT and AST levels of BGZ treated and untreated groups (receiver operating characteristic (ROC) ≥ 0.9).

**Conclusions** Yin$_{syn}$ and Yang$_{syn}$ are the predisposed syndromes for BGZ to exert liver damage and liver protection respectively, which are mainly related to the regulation of amino acid metabolism, lipid metabolism, energy metabolism, and metabolism of cofactors and vitamins. The results further suggest that attention should be paid to the selection of predisposed populations when using drugs related to the regulation of energy metabolism, and the Yin$_{syn}$/Yang$_{syn}$ animal models based on the theory of TCM syndromes may be a feasible method for identifying the susceptible population to receive TCM.

**Keywords** *Psoraleae Fructus*, Liver injury, Predisposed individual, Metabolomics, Transcriptomics

## Introduction

Drug-induced liver injury (DILI) refers to one of the most common and serious adverse drug reactions induced by various prescription or non-prescription chemical drugs, biological agents, traditional Chinese medicine (TCM), natural medicine, health care products, dietary supplements and their metabolites and even excipients, which can lead to acute liver failure or even death [1]. Due to the lack of drug-specific biomarkers, the diagnosis of DILI mainly depends on clinical judgment and exclusion of other liver diseases, and then through the causal relationship assessment to determine the degree of association between liver injury and suspected drugs [2]. Thus, the lack of evidence-based and reliable diagnostic tools has always been one of the prominent problems in the clinical diagnosis, treatment, and research of DILI. However, the proportion of DILI caused by traditional Chinese herbs and dietary supplements has increased year by year [3, 4]. This is particularly noticeable for non-toxic TCM such as *Polygonum multiflorum Thunb.*[5] and *Psoralea corylifolia* Linn (BGZ) [6], which have been used for thousands of years in China. This phenomenon is causing great confusion for doctors and patients. Thus, it is particularly critical to find the factors that induce DILI (especially DILI caused by TCM) and the specific biomarkers that characterize DILI.

DILI usually involves two factors, the "drug" and the "host" [7]. For drug factors, Chen et al. constructed a "role-of-two" model [8] and modified the version used [9]. The model enhanced the ability to predict whether a drug will cause DILI, but it was unable to fully explain individual differences in drug usage. Therefore, it cannot be used to predict individuals who are predisposed to DILI. Host factors are also important in understanding the susceptibility to DILI. Host factors that are generally recognized by modern research include hosts who carry specific HLA genes or the immune homeostasis of the host [9]. As reported in recent years, liver damages induced by *Polygonum multiflorum* Thunb., Green Tea, and Kampo products (Japanese traditional medicines), etc. are closely related to *HLA-B\*35:01* [10–12], while liver damage induced by flucloxacillin, pazopanib, abacavir, etc. are closely related to *HLA-B\*57:01* [13–17]. Screening susceptible genes and identifying susceptible populations are important methods to prevent the occurrence of liver injury caused by TCM. However, up to now, most of the hepatotoxicity of TCM has not been found in susceptible genes, and even if the susceptible gene is found, it does not necessarily represent that the person carrying the susceptible gene will have a specific liver injury when taking the TCM.

Actually, the identification of susceptible genes or populations is similar to the "*therapy with syndrome differentiation*" of TCM, both of which are based on identifying drug-susceptible populations for rational medication use. However, for TCM theory, in addition to the correct understanding of medicine, it is also necessary to correctly identify TCM syndromes that summarize the pathological changes of the body at a certain stage of disease development based on TCM theory. TCM treatment requires "*therapy with syndrome differentiation*". Symptomatic treatment can result in a better therapeutic effect, otherwise, it can aggravate the disease process and induce new diseases. Therefore, it may be feasible to explore the predisposition of individuals to TCM liver injury based on TCM syndrome theory which may provide a reference for other similar studies on the hepatotoxicity of TCM.

BGZ, the dried mature fruit of the leguminous plant *Psoralea corylifolia* Linn, is widely used in Asia and has

Zhang *et al. Chinese Medicine*     (2023) 18:102

Page 3 of 23

been used for many years in China to treat symptoms such as impotence, nocturnal emission, enuresis, frequent urination, cold aching in the lower back and knees, kidney deficiency, and premature ejaculation [18]. BGZ has definite pharmacological effects, such as anti-tumor, anti-oxidation, antibacterial, anti-inflammatory, anti-depression, estrogen level regulation, bone growth promotion, nerve protection, and influence on the liver [19]. Its active ingredients, psoralen, and 5-methoxypsoralen, have become commonly used in the clinical treatment of vitiligo and psoriasis [20, 21]. In addition, BGZ and its related compounds are also commonly used in health food and dietary supplements. However, in recent years, BGZ and its related compound preparations Zhuanggu Guanjie Pill and Xianling Gubao Capsules were reported to induce DILI in China [6, 22–24]. The BGZ-induced liver injury also occurred in South Korea [25].

Although some studies have confirmed that BGZ and some of its components have hepatotoxicity [6, 26, 27], these studies only focused on the drug itself and did not consider the host factors that induced DILI. Accordingly, by integrating the basic disease characteristics of the population treated with BGZ, our previous study found that most BGZ-induced DILI patients had osteoporosis, psoriasis, osteoarthritis, and other basic diseases related to immune activation [28], and such diseases were found to be closely related to the imbalance of kidney-yang deficiency syndrome (Yang$_{syn}$) and kidney-yin deficiency syndrome (Yin$_{syn}$) according to TCM diagnosis [29–31]. The ancient TCM medicine book "*Lei Gong Concocting (Paozhi) Theory*" also recorded during the Northern and Southern Dynasties in China that people with "asthenic yin causing excessive pyrexia" should avoid taking BGZ. Thus, the BGZ-induced DILI may be related to its inappropriate symptomatic treatment. However, whether it has a causal relationship with the imbalance of Yang$_{syn}$ and Yin$_{syn}$ in the body remains unclear.

According to the diagnostic criteria of TCM syndromes [32], patients with Yang$_{syn}$ generally have low body temperature, loose stools, and less drinking and urine, while patients with Yin$_{syn}$ generally have high body temperature, dry stool, polydipsia, and polyuria. In addition, some studies have found that the expression of cAMP in patients with Yang$_{syn}$ decreased [33, 34], while the expression of cAMP in patients with Yin$_{syn}$ increased [34, 35]. Accordingly, continuously administered high doses of exogenous glucocorticoid (GC) (e.g., hydrocortisone) [36] or thyroxine + reserpine [37] in rats were used to build the models of Yang$_{syn}$ and Yin$_{syn}$, respectively. The changes in behavioral signs and cAMP levels in the above animal models are similar to the clinical patients with the corresponding syndromes and have been generally recognized and adopted by experts in the related

fields of TCM. With a good description of the changes in the metabolic characteristics of endogenous metabolites and the differential expression changes of a series of functional genes in organisms, metabolomics and transcriptomics have been successfully applied to screen various diseases and their metabolic or gene profile changes in drug intervention [38, 39]. This study constructed Yang$_{syn}$ and Yin$_{syn}$ animal models to evaluate whether the liver damage induced by BGZ is related to its non-symptomatic use and the possible susceptible individual characteristics.

## Experiment

### Chemicals and reagents

Hydrocortisone succinate sodium was provided by Tianjin Biochemical Pharmaceutical Co., Ltd. (Tianjin, China). Thyroxine and reserpine were provided by Shanghai MACKLIN Technology Co., Ltd. (Shanghai, China). Alanine aminotransferase (ALT), aspartate aminotransferase (AST), serum creatinine (Scr), lactate dehydrogenase (LDH), and Na$^+$-K$^+$-ATP$_{ase}$ tests were purchased from Jiancheng Biological Technology, Co., Ltd. (Nanjing, China). Cyclic adenosine monophosphate (cAMP) was purchased from Mlbio Biotechnology Co., Ltd. (Shanghai, China).

### BGZ Preparation

BGZ was purchased from the Anhui Puren Herbal Pieces Co., Ltd. (Anhui, China) and authenticated by Professor Xiaohe Xiao of the Institute of Hepatology, Fifth Medical Center, PLA General Hospital (Beijing, China). In addition, BGZ was crushed and filtered through 200 mesh sieves and then suspended in 0.5% sodium carboxymethyl cellulose (CMC-Na) for administration.

### Animal maintenance and treatment

Male Sprague–Dawley rats (180–200 g) were obtained from the SPF Biotechnology Co. Ltd. (License No. SCXK20190010, Beijing, China), and housed in the Laboratory Animal Center of the Fifth Medical Center, Chinese PLA General Hospital (animal ethics committee approval No. YFYDW2020017). All rats were raised under specific pathogen-free conditions under a 12 h light/dark cycle, with free access to adequate food and water. All animals were fed adaptively for 1 week before starting the experiments.

The rats were randomly divided into six separate groups (N=8) as follows: Control group (CON), BGZ group (BGZ), kidney-yang deficiency syndrome group (Yang$_{syn}$), kidney-yang deficiency syndrome-treated with BGZ group (Yang$_{syn}$+BGZ), kidney-yin deficiency syndrome group (Yin$_{syn}$); kidney-yin deficiency syndrome-treated with BGZ group (Yin$_{syn}$+BGZ). Rats in

Zhang *et al. Chinese Medicine*        (2023) 18:102

Page 4 of 23

the BGZ-related treatment groups were consecutively administered intragastrically with BGZ suspension for 21 consecutive days, while the CON, Yang$_{syn}$, and Yin$_{syn}$ groups received the same volume of 0.50% CMC-Na solution for the same amount of time. The changes in body weight were recorded before the end of the experiment. From the 8th day of administration, the Yang$_{syn}$ and Yang$_{syn}$+BGZ group rats were given 25 mg/kg hydrocortisone subcutaneously once a day for 14 consecutive days to prepare the Yang$_{syn}$ model [36]. From the 15th day of administration, the Yin$_{syn}$ and Yin$_{syn}$+BGZ group rats were given thyroxine (16 mg/mL) and reserpine (1 mg/mL) at the dosage of 0.5 mL/100 g via gastric perfusion once a day for 7 consecutive days to prepare the Yin$_{syn}$ model [37]. The CON and the BGZ groups were given the same volume of 0.50% CMC-Na solution.

### Urine volume, water intake, anal temperature, fecal water content changes

According to the diagnostic criteria of TCM syndromes [32], patients with Yang$_{syn}$ generally have low body temperature, loose stools, less drinking, and less urine, while patients with Yin$_{syn}$ generally have high body temperature, dry stool, polydipsia, and polyuria. Thus, the anal temperature, fecal water content, 24 h drinking water volume, and 24 h urine volume before the last administration were selected as the criteria to evaluate whether the models of Yang$_{syn}$ and Yin$_{syn}$ were successfully constructed as the previous reports [40, 41].

### Blood collection, organ index, and tissue preparation

After the experiment, all animals were anesthetized with 2% pentobarbital sodium. Blood samples with and without anticoagulants were collected, and the liver, kidney, adrenal gland, testis, spleen, brain, lung, and heart were weighed immediately after sacrifice to calculate the organ index. Partial liver tissue was collected for histological examination and the remaining liver was quickly frozen with liquid nitrogen and stored at $-80$ °C until needed.

### Serum biochemistry and histopathological analysis

After centrifugation (3500 rpm, 10 min, 4 °C), serum biochemistry of ALT, AST, Scr, LDH, Na$^+$-K$^+$-ATP$_{ase}$, and cAMP were determined according to the microplate assay kit instructions, the left hepatic lobe was fixed with 4% paraformaldehyde for 48 h, embedded in wax, and sectioned at approximately 5 μm for Hematoxylin and Eosin (HE) pathological staining analysis.

### RNA sequence analysis and data processing

Total RNA was extracted from liver tissues using Trizol reagent (Invitrogen, USA) according to the manufacturer's protocol, and genomic DNA was removed using DNase I (TaKara). RNA quality was assessed with a Bioanalyzer 2100 (Agilent) and measured with a NanoDrop 2000 spectrophotometer. Only a high-quality RNA sample (OD$_{260/280}$ = 1.8~2.2, OD$_{260/230}$ ≥ 2.0, RNA integrity number (RIN) ≥ 6.5, 28 S:18 S ≥ 1.0, > 1 μg) was used to construct the sequencing library. RNA-seq transcriptome libraries were prepared using a TruSeqTMRNA sample preparation kit from Illumina (San Diego, CA) and sequenced with the Illumina HiSeq xten/NovaSeq 6000 sequencer under standard protocols. All samples had a Q30 (bases of Q ≥ 30 /all bases of sequencing) of > 91%. Sequence readers were trimmed and quality controlled using SeqPrep (https://github.com/jstjohn/SeqPrep) and Sickle (https://github.com/najoshi/sickle) with default parameters and aligned to the reference genome through the orientation mode using hierarchical indexing for spliced alignment of transcripts 2 (HISAT2) [42]. Messenger RNA levels were quantified using RNA-Seq by Expectation-Maximization (RSEM) (http://deweylab.biostat.wisc.edu/rsem/) [43]. Differentially expressed genes (DEGs) were identified as those with fold change (FC) ≥ 1.5, (FC) ≤ 0.67, and *Padjust < 0.05* (DESeq2) [44]. Furthermore, Gene Ontology (GO, http://www.geneontology.org) functional enrichment and Kyoto Encyclopedia of Genes and Genomes (KEGG, http://www.genome.jp/kegg/) pathway analysis carried out by Goatools (https://github.com/tanghaibao/Goatools) and KOBAS (http://kobas.cbi.pku.edu.cn/home.do) were performed to determine significant GO terms and pathways associated with the DEGs [45]. Pathways with *Padjust < 0.05* were considered potential target pathways.

### Reverse transcription-quantitative polymerase chain reaction (RT-qPCR)

Liver tissue RNA was extracted by the Tissue RNA Purification Kit Plus (RN002plus, ES Science, China) and reverse-transcribed into cDNA using the Fast All-in-One RT Kit (RT001, ES Science, China) according to the manufacturer's instructions. The qPCR of aldehyde dehydrogenase 1 family member B1 (Aldh1b1), galectin 5 (Lgals5), solute carrier family 25 member 25 (Slc25a25), Pim-3 proto-oncogene, serine/threonine kinase (Pim3), and out at first (Oaf) were quantified by the SYBR Green PCR master mix (RN002plus, ES Science, China) with the QuantStudio 6 Flex PCR System (Applied Biosystems, USA). The amplification parameters were set according to the standard protocol. Primer sequences used in this study are shown in Additional

Zhang *et al. Chinese Medicine*      (2023) 18:102

Page 5 of 23

file 1: Table S1. Relative gene expression was calculated using the $2^{-\triangle\triangle Ct}$ method $2^{-\triangle\triangle Ct}$ [46].

### Liver sample processing

The liver was homogenized with normal saline at 1:1 (1 g:1 mL) using a homogenizer. The 300 uL homogenized sample and 900 uL methanol were mixed and vortexed for 30 s. The supernatant was centrifuged at 12,000 r/min for 10 min and concentrated to dry using a vacuum centrifugal concentrator. Then 100 uL methanol was added for redissolving and centrifuged at 13,000 r/min for 10 min. Finally, a 4 uL supernatant was taken out for UPLC-QTOF/MS (Waters, Manchester, UK) detection.

### UPLC-QTOF/MS analysis and data processing

Metabolic profiling analysis of the biofluids was performed using the Waters Xevo G2-XS QTOF/MS (Waters, Manchester, UK). An analytical Acquity UPLC HSS T3 C18 column (temperature 30 ℃) was injected with 4 μL aliquots of each sample. For positive electrospray ionization source (ESI+) and negative electrospray ionization source (ESI-) analysis, samples were isolated using a 30 min linear gradient of solvent A (water spiked with 0.1% formic acid) and solvent B (acetonitrile spiked with 0.1% formic acid) as mobile phases. The flow rate was fixed at 0.30 mL/min. For each sample, 10 μL was drawn as a quality control sample to ensure that the system was stable and the analyses were repeatable. Every 20th sample was injected with the control sample and subsequently analyzed. Masslynx software (v4.1, Waters Corp.) and Progenesis QI (v. 2.4, Waters Technologies, UK) were used for identifying the original mass spectral data and normalizing the total ion intensity of each chromatogram to acquire a data matrix containing the m/z value, retention time (RT), and normalized peak area. SIMCA-P 14.1 software (Umetrics, Umea, Sweden) was used for principal component analysis (PCA) and orthogonal partial least-squares discriminant analysis (OPLS-DA). The PCA score chart was used to show the natural interrelation of observation results. Variable importance in the projection (VIP) ≥ 1 and *P < 0.05* were selected as potential metabolites. Online metabolic databases including the Human Metabolome Database (HMDB) (http://www.hmdb.ca/) and Kyoto Encyclopedia of Genes and Genomes (KEGG) (https://www.genome.jp/kegg/) were combined with exact masses and secondary ion mass spectrometry of the metabolites acquired through Progenesis QI to identify the differential metabolites.

### Integrated analysis

Cytoscape 3.8.0 (https://js.cytoscape.org/) is a visualization tool for exploring biomedical networks composed of compounds, genes, and other types of interactions [47]. MetScape (http://MetScape.ncibi.org) is a plugin of Cytoscape that allows users to construct and analyze gene and compound networks, and identify and visualize enriched pathways changes in expression profiling data and metabolite data [48]. The data obtained for differentially abundant metabolites and DEGs from rats in the Yang$_{syn}$/Yin$_{syn}$ and corresponding BGZ-treated groups were imported into Metscape to obtain a global understanding of gene and metabolic changes to assess the underlying mechanisms of Yin$_{syn}$/Yang$_{syn}$-associated differential responses to BGZ in rat models, respectively.

### Statistical analysis

Statistical analysis was performed with Prism 8.0 (GraphPad Software, San Diego, CA). All results are expressed as mean ± SD. A one-way analysis of variance (ANOVA) was used to statistically analyze the multiple-group analysis. The student's t-test was used to statistically analyze the receiver operating characteristic (ROC) curve analysis. The significance threshold was set at *P < 0.05*.

## Results

### Effect of BGZ treatment on the changes in body weight, anal temperature, water intake, urine volume, fecal water content, and cAMP in Yin$_{syn}$ and Yang$_{syn}$ model rats

As shown in Fig. 1, compared with the CON group, the levels of weight, anal temperature, water intake, urine volume, and fecal water content in the BGZ group had no obvious changes, but the levels of anal temperature, urine volume, and cAMP were all significantly decreased (all *P < 0.05*) and accompanied with the significantly increased fecal water content (*P < 0.01*) in the Yang$_{syn}$ group, while the levels of anal temperature, water intake, urine volume, and cAMP were all significantly increased (all *P < 0.05*) and accompanied with the significantly decreased fecal water content (*P < 0.05*) in the Yin$_{syn}$ group. The change trends of behavioral characteristics and cAMP in the above-mentioned Yang$_{syn}$/Yin$_{syn}$ model rats were similar to the definition of Yang$_{syn}$/Yin$_{syn}$ in the diagnostic criteria of TCM syndromes. Under the intervention of BGZ, the levels of anal temperature, urine volume, and cAMP were all significantly increased (all *P < 0.05*) and accompanied by the significantly decreased

Zhang *et al. Chinese Medicine*     (2023) 18:102

Page 6 of 23
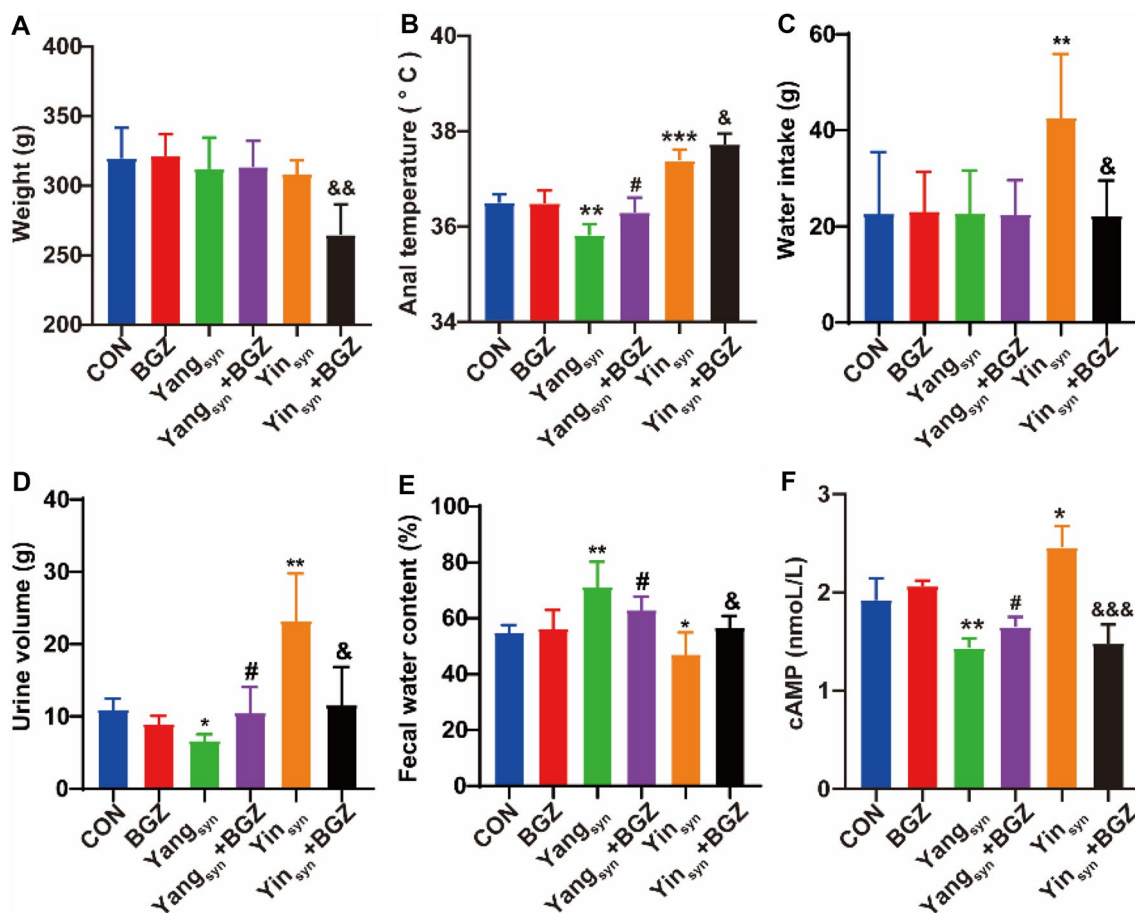


**Fig. 1** Effect of BGZ treatment on changes in body weight, anal temperature, water intake, urine volume, fecal water content, and cAMP (N = 6 ~ 8). Weight (**A**), Anal temperature (**B**), Water intake (**C**), Urine volume (**D**), Fecal water content (**E**), and cAMP (**F**). *$P < 0.05$, **$P < 0.01$, ***$P < 0.001$, compared with CON group; #$P < 0.05$, compared with Yang$_{syn}$ group; &$P < 0.05$, &&$P < 0.01$, compared with Yin$_{syn}$ group

fecal water content ($P < 0.05$) in the Yang$_{syn}$+BGZ group compared with the Yang$_{syn}$ group, while the levels of weight, water intake, urine volume, and cAMP were all significantly decreased (all $P < 0.05$) and accompanied with the significantly increased anal temperature and fecal water content (both $P < 0.05$) in the Yin$_{syn}$+BGZ group compared with the Yin$_{syn}$ group.
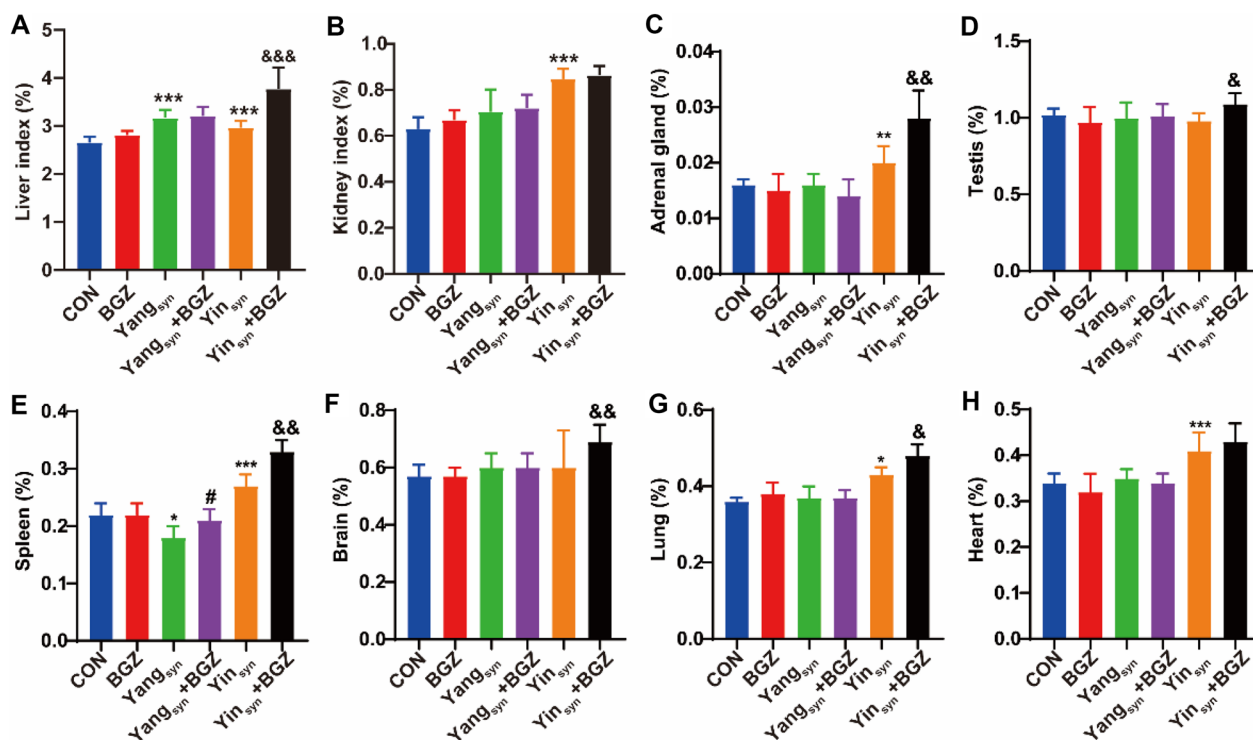
### Effect of BGZ treatment on the changes in organ indexes in Yin$_{syn}$ and Yang$_{syn}$ model rats

As shown in Fig. 2, compared with the CON group, all organ indexes in the BGZ group had no obvious changes, while the liver index was significantly increased ($P < 0.001$) and accompanied by the significantly increased spleen index ($P < 0.05$) in the Yang$_{syn}$ group, but the organ indexes of the liver, kidney, adrenal gland, spleen, lung, and heart in the Yin$_{syn}$ group were all significantly increased (all $P < 0.05$). Under the intervention of BGZ, the spleen index in the Yang$_{syn}$+BGZ group was significantly increased ($P < 0.05$) compared with the Yang$_{syn}$ group, while all organ

indexes (except for kidney and heart) in the Yin$_{syn}$+BGZ group were significantly increased compared with the Yin$_{syn}$ group (all $P < 0.05$).

### Effect of BGZ treatment on the serum levels of ALT, AST, Scr, and liver histopathological changes in Yin$_{syn}$ and Yang$_{syn}$ model rats

Serum ALT, AST, and Scr, which are well-recognized markers of various types of liver and kidney damage, were used for the analysis. As for liver function (Fig. 3A–B), there were no obvious changes in the levels of ALT and AST between the BGZ group and the CON group. In contrast, the levels of ALT and AST in the Yang$_{syn}$ group increased prominently, while BGZ significantly reversed the phenomena (all $P < 0.05$). Though the AST level in the Yin$_{syn}$ group was significantly increased ($P < 0.01$), there was no obvious change in the levels of AST between the Yin$_{syn}$+BGZ group and the Yin$_{syn}$ group, while the ALT level was significantly increased after administration of BGZ in the Yin$_{syn}$+BGZ group

**Fig. 2** Effect of BGZ treatment on changes in organ indexes (N = 8). Liver (**A**), Kidney (**B**), Adrenal gland (**C**), Testis (**D**), Spleen (**E**), Brain (**F**), Lung (**G**) and Heart (**H**). *$P < 0.05$, **$P < 0.01$, ***$P < 0.001$, compared with CON group; #$P < 0.05$, compared with Yang$_{syn}$ group; &$P < 0.05$, &&$P < 0.01$, &&&$P < 0.001$, compared with Yin$_{syn}$ group

($P < 0.001$), illustrating that there was a certain risk of liver injury in rats with Yin$_{syn}$ after administration of BGZ. As for kidney function (Fig. 3C), no significant Scr changes were found in almost all groups except for the Yin$_{syn}$ group ($P < 0.001$). Combined with the changes in the kidney organ index, it revealed that BGZ may have no obvious renal toxicity in rats with Yang$_{syn}$ or Yin$_{syn}$. As shown in Fig. 3D, the liver sections of the CON group showed normal hepatocyte structures. The liver samples from BGZ-treated rats were almost indistinguishable from normal rats. The liver samples from the Yang$_{syn}$ group exhibited hepatocyte focal necrosis, loss of central vein intima, and inflammatory cell infiltration in portal vein areas, while the above symptoms were alleviated in the Yang$_{syn}$+BGZ group. The liver samples from the Yin$_{syn}$ group exhibited slight inflammatory infiltration in the portal area but no evident hepatocyte injury, while the hepatocyte focal necrosis and inflammatory cell infiltration were aggravated in the Yin$_{syn}$+BGZ group. Combined with the levels of ALT, AST, liver index, and liver pathological examination, it was suggested that BGZ has a preferable liver protection effect on rats with Yang$_{syn}$ and a certain risk of liver injury effect on rats with Yin$_{syn}$.

## DEGs alterations of BGZ treatment in Yin$_{syn}$ and Yang$_{syn}$ model rats

To reveal the mechanism of different therapeutic effects of BGZ on Yin$_{syn}$ and Yang$_{syn}$ rats, liver gene expression profiles were obtained from the CON, BGZ, Yang$_{syn}$, Yang$_{syn}$+BGZ, Yin$_{syn}$, and Yin$_{syn}$+BGZ groups using RNA-Seq analysis. As shown in Fig. 4A, compared with the CON group, BGZ barely influenced the gene expression with only 4 DEGs increased and 5 DEGs decreased, while 439 up-regulated DEGs and 652 down-regulated DEGs were found in the Yang$_{syn}$ group, and 508 up-regulated DEGs along with 847 down-regulated DEGs were found in the Yin$_{syn}$ group. Compared to the Yang$_{syn}$ group, the number of up-regulated and down-regulated DEGs decreased to 59 and 43 by BGZ treatment, respectively (Additional file 1: Table S2), while for the Yin$_{syn}$ group, the number of up-regulated and down-regulated DEGs decreased to 11 and 17 by BGZ treatment, respectively (Additional file 1: Table S3). To further display the above differences in DEGs more intuitively, heatmaps were constructed based on relative abundance (Fig. 4B, C).

Zhang *et al. Chinese Medicine*     (2023) 18:102

Page 8 of 23
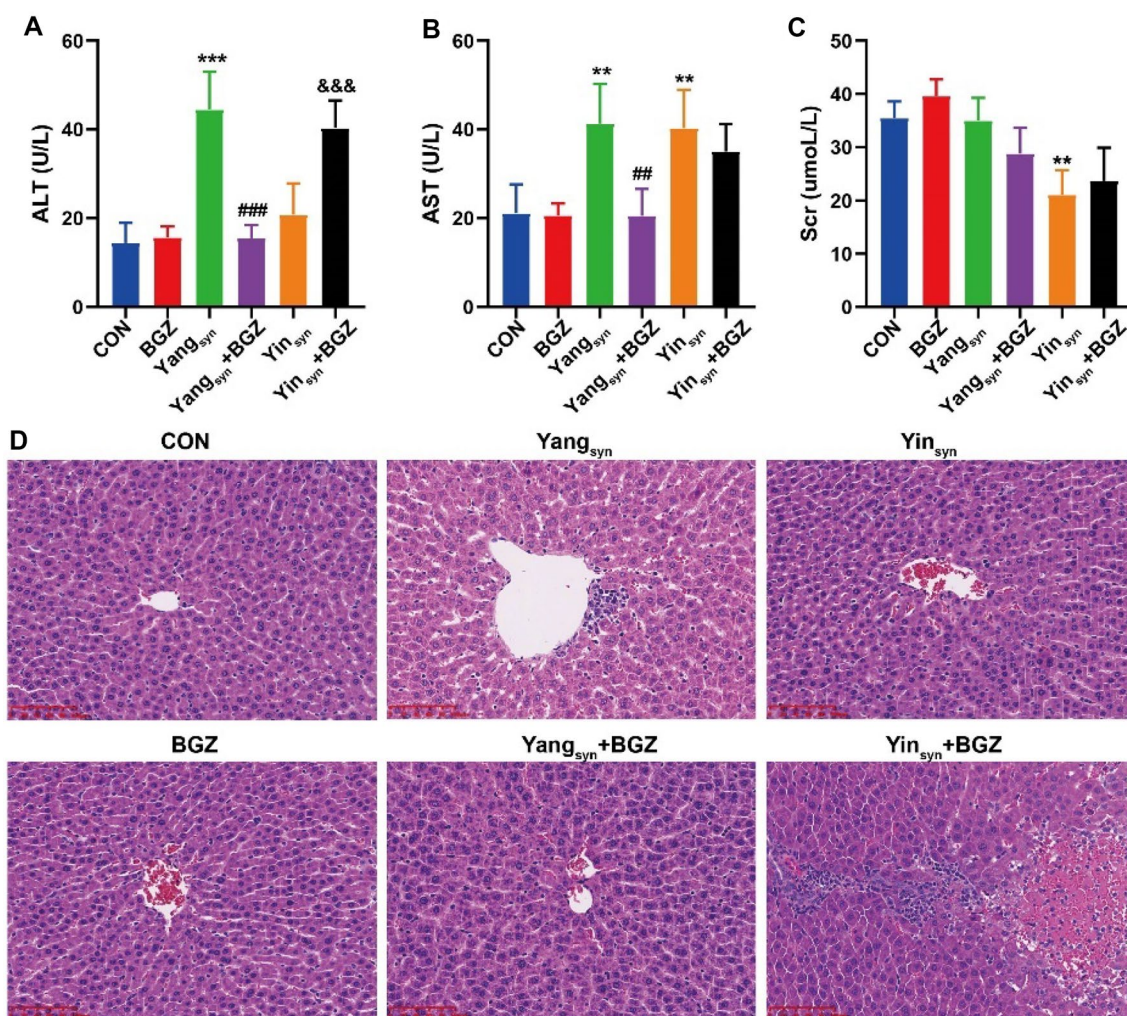


**Fig. 3** Effect of BGZ treatment on serum biochemistry and HE staining (N = 6 ∼ 8). Serum ALT (**A**), AST (**B**), and Scr (**C**) activity. \*\**P < 0.01*, \*\*\**P < 0.001*, compared with CON group; ##*P < 0.01*, ###*P < 0.001*, compared with Yang$_{syn}$ group; &&&*P < 0.001*, compared with Yin$_{syn}$ group. (**D**) Typical histopathological section photographs of rat liver specimens for HE analysis (Scale bar, 100 μm)

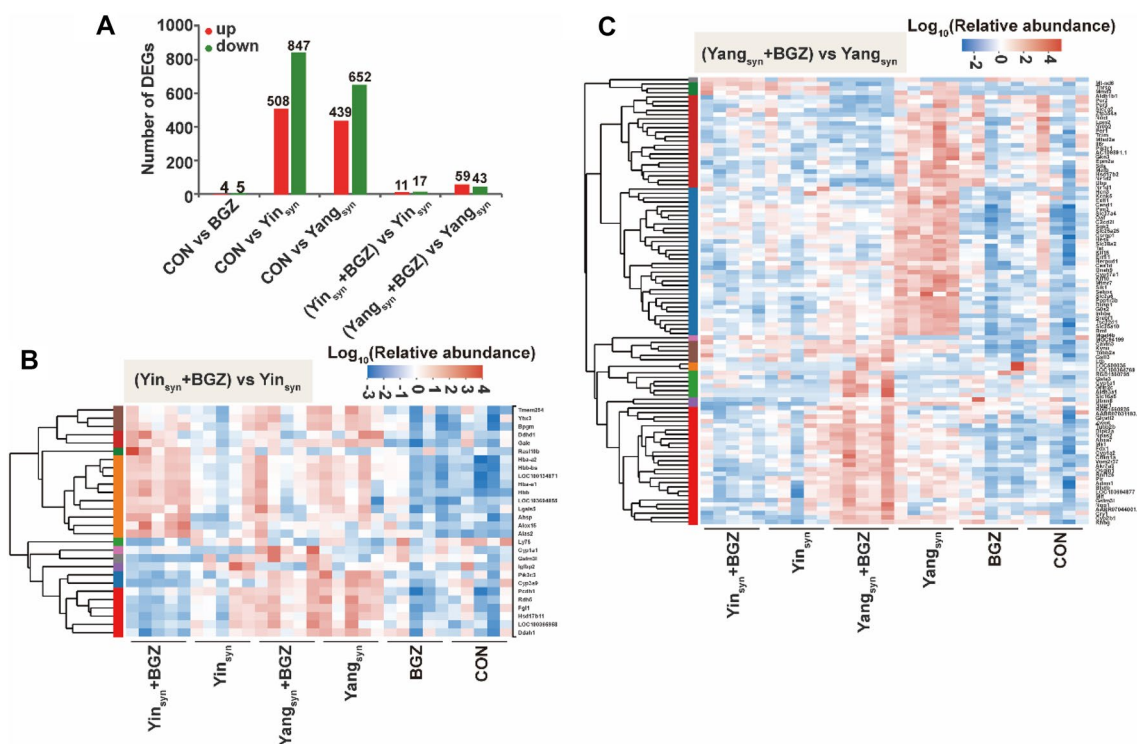## Correlation Analysis of the relative abundance of DEGs and the levels of serum biochemistry (ALT and AST)

By analyzing the correlations between serum biochemistry (ALT and AST) and DEGs changed using BGZ in Yin$_{syn}$ and Yang$_{syn}$ rats (Fig. 5), the results demonstrated that 36 DEGs, including 34 positive DEGs and 2 negative DEGs, were significantly correlated with ALT, and 12 DEGs, including 9 positive DEGs and 3 negative DEGs, were significantly correlated with AST. Among them, hyperpolarization-activated cyclic nucleotide-gated potassium channel 3 (Hcn3), aldehyde dehydrogenase 1 family member B1 (Aldh1b1), galectin 5 (Lgals5), solute carrier family 25 member 25 (Slc25a25), Pim-3 proto-oncogene, serine/threonine kinase (Pim3), and out at first (Oaf) were all significantly positively correlated with ALT and AST, and LOC100364769 was significantly negatively correlated with ALT and AST. The detailed relationship

between DEGs and serum biochemistry (ALT and AST) was shown in Additional file 1: Table S4.

### ROC curve analysis of DEGs and RT-qPCR verification

To further explore the diagnostic efficacy of DEGs, a ROC curve analysis was performed using GraphPad Prism software (version 8.01). The results revealed that 22 DEGs could be better discriminated between the Yang$_{syn}$+BGZ group and Yang$_{syn}$ group, and 10 DEGs had better discrimination between the Yin$_{syn}$+BGZ group and Yin$_{syn}$ group (all the areas under the curve (AUC) of the ROC curves ≥ 0.9 and *P < 0.05*) (Additional file 1: Fig. S1). Venn analysis showed the ROC results of DEGs and their correlation with the levels of ALT and AST between the Yang$_{syn}$+BGZ group and Yang$_{syn}$ group (Fig. 6A), revealing that Aldh1b1, Slc25a25, Pim3, and Oaf can be used as potential

Zhang *et al. Chinese Medicine*    (2023) 18:102

Page 9 of 23



**Fig. 4** Transcriptomic alterations of BGZ treatment on Yin_syn and Yang_syn rats (N = 5). **A** The number of DEGs compared with each group. The red color represents up-regulated genes and the green color represents down-regulated genes. **B** Heatmap showing the intersection of DEGs between the Yin_syn+BGZ group and the Yin_syn group. **C** Heatmap showing the intersection of DEGs between the Yang_syn+BGZ group and the Yang_syn group
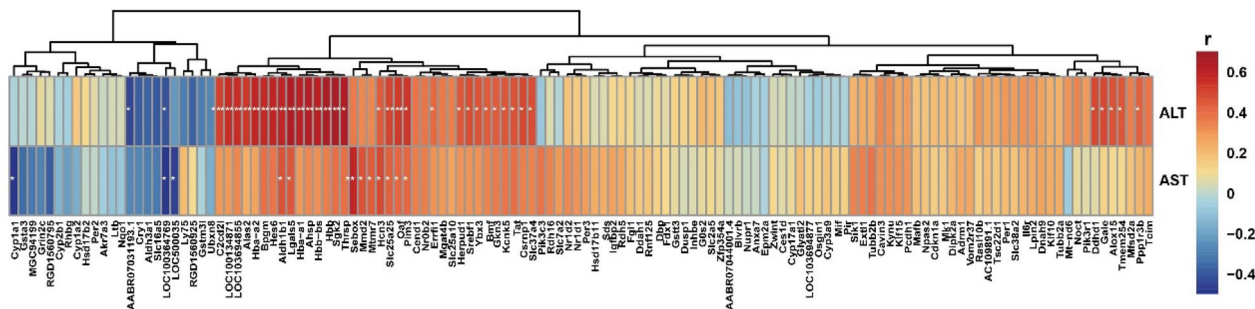


**Fig. 5** The relationship between the relative abundance of DEGs and the levels of serum biochemistry (ALT and AST) (N = 5). Color depth represents correlation strength, the red color represents positive correlation, and the blue color represents negative correlation. *$P < 0.05$, **$P < 0.01$, ***$P < 0.001$

biomarkers for the treatment of Yang_syn (Fig. 6B–E). Venn analysis also showed the ROC results of DEGs and their correlation with ALT and AST between the Yin_syn+BGZ group and Yin_syn group (Fig. 6F), revealing that Lgals5 may be used as a potential biomarker for the treatment of Yin_syn (Fig. 6G). RT-qPCR verification of the above marker genes revealed that, as shown in Fig. 6H–L, compared with the CON group, the expression of Aldh1b1, Slc25a25, Pim3, Oaf, and Lgals5 in rats with Yang_syn were all significantly increased (all

$P < 0.05$), while the levels of Aldh1b1 and Lgals5 were both decreased (both $P < 0.05$) and accompanied with the significantly increased Slc25a25 and Pim3 (both $P < 0.05$) in the Yin_syn group. Under BGZ intervention, the levels of Aldh1b1, Slc25a25, Pim3, Oaf, and Lgals5 were all significantly decreased in the Yang_syn+BGZ group compared with the Yang_syn group (all $P < 0.001$), while only Lgals5 was significantly increased in rats with Yin_syn+BGZ compared with the Yin_syn group ($P < 0.05$).

Zhang *et al. Chinese Medicine*    (2023) 18:102

Page 10 of 23
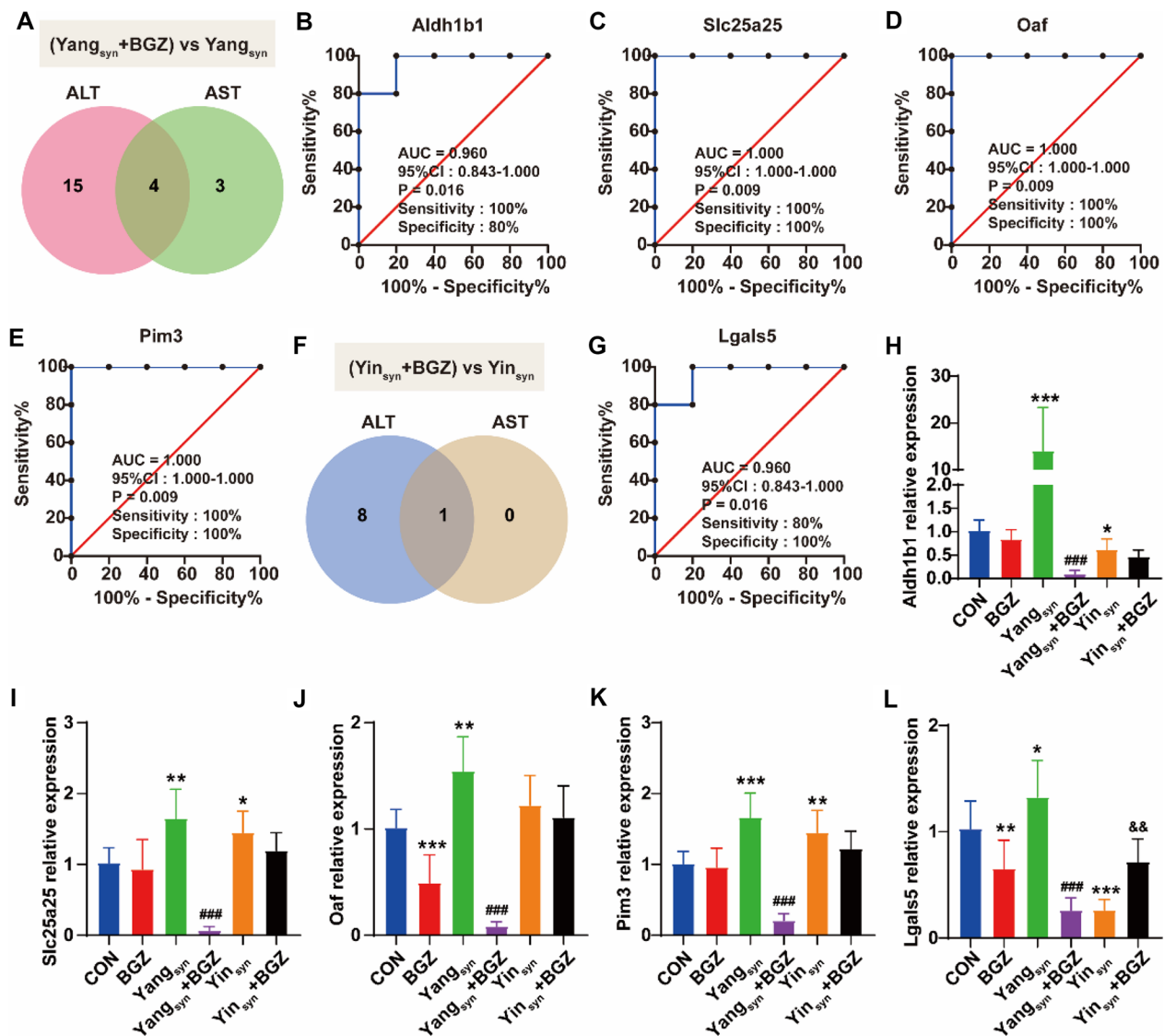


**Fig. 6** ROC analysis of DEGs associated with ALT and AST expression and RT-qPCR verification. **A** Venn diagram showing the number of DEGs associated with the levels of ALT and AST under ROC ≥ 0.90 between the Yang$_{syn}$+BGZ group and the Yang$_{syn}$ group. **B–E** ROC curves of DEGs associated with the levels of ALT and AST under ROC ≥ 0.90 between the Yang$_{syn}$+BGZ group and Yang$_{syn}$ group, Aldh1b1 (**B**), Slc25a25 (**C**), Oaf (**D**), and Pim3 (**E**). **F** Venn diagram showing the number of DEGs associated with the levels of ALT and AST under ROC ≥ 0.90 between the Yin$_{syn}$+BGZ group and the Yin$_{syn}$ group. **G** ROC curves of Lgals5 between the Yin$_{syn}$+BGZ group and the Yin$_{syn}$ group. **H–L** The mRNA expression of Aldh1b1 (**H**), Slc25a25 (**I**), Oaf (**J**), Pim3 (**K**), and Lgals5 (**L**). $*P < 0.05$, $**P < 0.01$, $***P < 0.001$, compared with CON group; $^{###}P < 0.001$, compared with Yang$_{syn}$ group; $^{\&\&}P < 0.01$, compared with Yin$_{syn}$ group

**GO and KEGG functional enrichment analysis of DEGs**

GO functional enrichment analysis found that 95 GOs (Additional file 1: Table S5) were significantly changed in the Yang$_{syn}$+BGZ group compared with the Yang$_{syn}$ group, such as GO:0009991 (response to extracellular stimulus), GO:0032922 (circadian regulation of gene expression), GO:0031667 (response to nutrient levels), and GO:0009892 (negative regulation of metabolic process), while 6 GOs including GO:0019825 (oxygen binding), GO:0020037 (heme-binding), GO:0046906 (tetrapyrrole binding), GO:0005833 (hemoglobin complex), GO:0005344 (oxygen carrier activity), and GO:0042743 (hydrogen peroxide metabolic process) were significantly changed in the Yin$_{syn}$+BGZ group compared with the Yin$_{syn}$ group. However, there is no intersection in the GO terms of regulating liver function in rats with
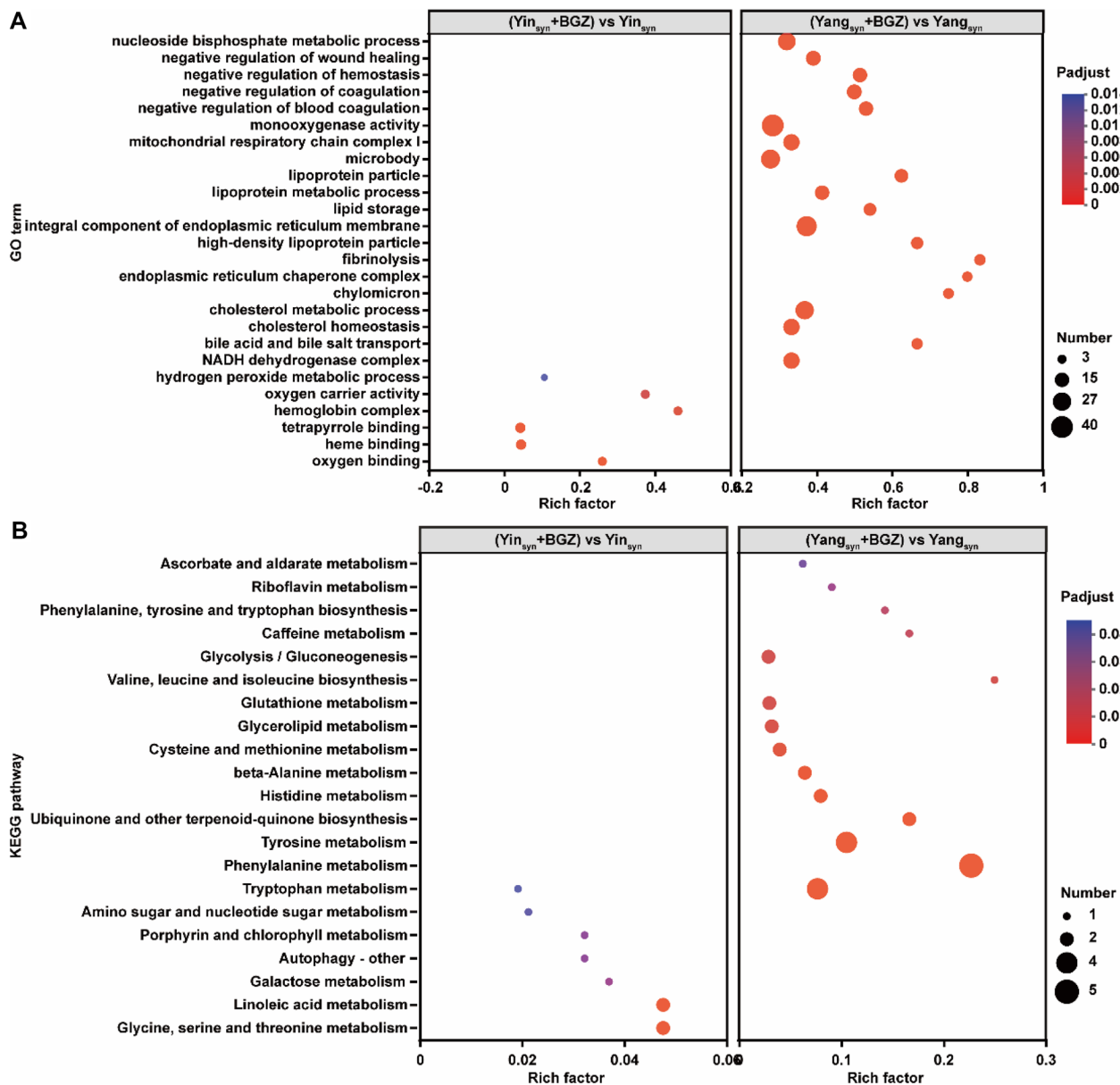
**Fig. 7** GO and KEGG functional enrichment pathways analysis of DEGs. **A** GO enrichment analysis. **B** KEGG enrichment analysis

Yang$_{syn}$/Yin$_{syn}$ by BGZ, Fig. 7A only displays the top 20 GO terms of the DEGs enrichment levels based on the value of *Padjust < 0.05*, respectively.

KEGG functional enrichment analysis found it mainly involves 15 pathways, including amino acid metabolism (phenylalanine metabolism, tyrosine metabolism, tryptophan metabolism, histidine metabolism, cysteine and methionine metabolism, valine, leucine and isoleucine biosynthesis, phenylalanine, tyrosine and tryptophan biosynthesis), carbohydrate metabolism (glycolysis/

gluconeogenesis, ascorbate and aldarate metabolism), lipid metabolism (glycerolipid metabolism), were significantly changed in the Yang$_{syn}$+BGZ group compared with the Yang$_{syn}$ group. while 7 pathways, including amino acid metabolism (tryptophan metabolism), carbohydrate metabolism (galactose metabolism), lipid metabolism (arachidonic acid metabolism), metabolism of cofactors and vitamins (porphyrin and chlorophyll metabolism), were significantly changed in the Yin$_{syn}$+BGZ group compared with the Yin$_{syn}$
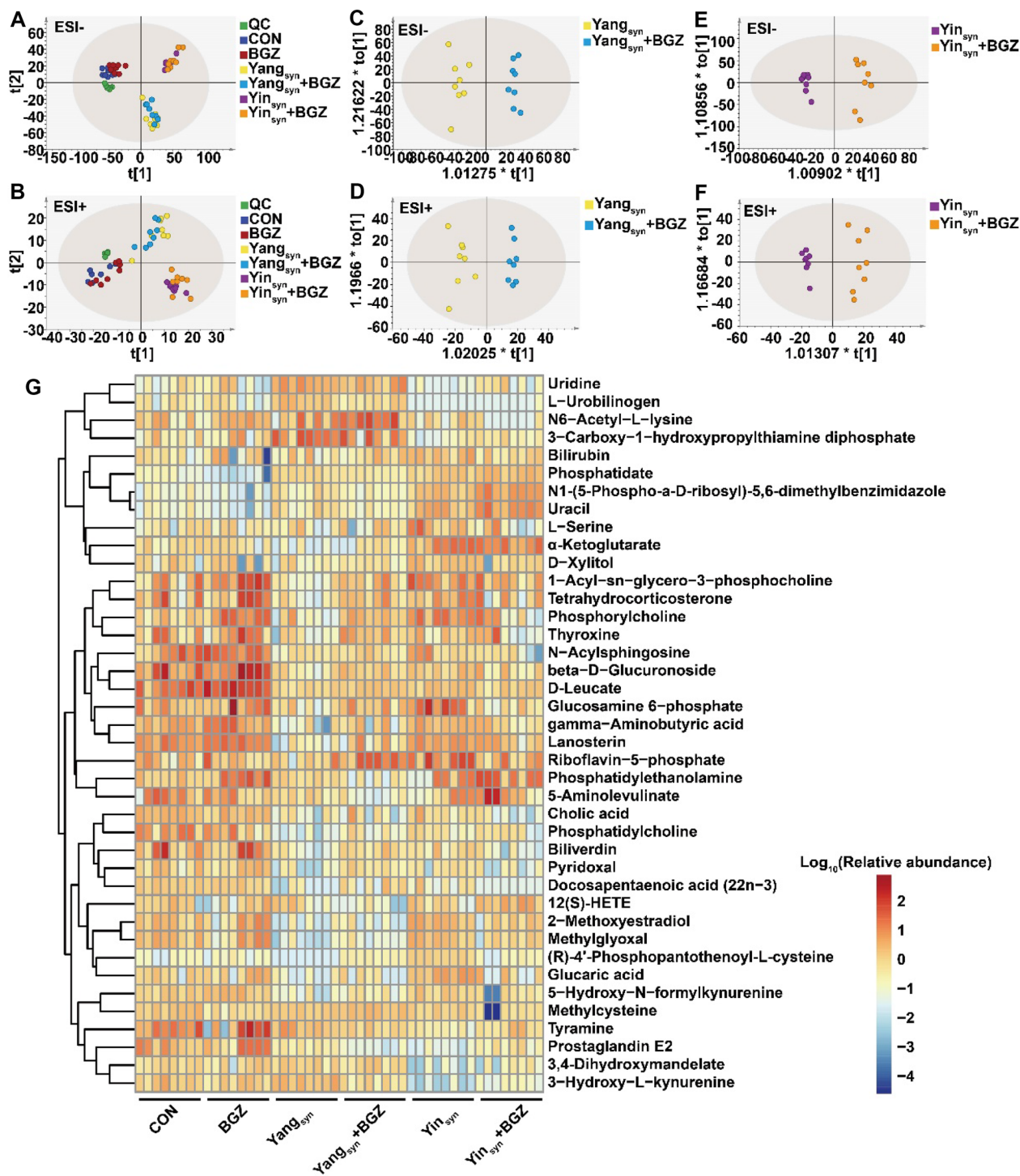
**Fig. 8** Metabolomic alterations of BGZ treatment on Yin$_{syn}$ and Yang$_{syn}$ rats (N = 8). **A**–**B** Scatter plot of liver metabolites in all groups determined by PCA in ESI- mode (**A**) and ESI + mode (**B**). **C**–**D** Scatter plot of liver metabolites between the Yang$_{syn}$+BGZ and Yang$_{syn}$ groups determined by OPLS-DA in ESI- mode (**C**) and ESI + mode (**D**). **E**–**F** Scatter plot of liver metabolites between the Yin$_{syn}$+BGZ and Yin$_{syn}$ groups determined by OPLS-DA in ESI- mode (**E**) and ESI + mode (**F**). **G** Heatmap of the metabolites identified. Color depth represents the variation trend of the relative abundance of metabolites, the red color represents up-regulated metabolites, and the blue color represents down-regulated metabolites

Zhang *et al. Chinese Medicine*     (2023) 18:102

Page 13 of 23

group. However, the KEGG pathway of BGZ regulating liver function in rats with Yang$_{syn}$/Yin$_{syn}$ has only one intersection (tryptophan metabolism). Figure 7B only shows the top 20 KEGG pathways of the DEGs enrichment degree according to the value of *Padjust < 0.05*, respectively.

## Metabolomic analysis of BGZ treatment in Yin$_{syn}$ and Yang$_{syn}$ model rats

As shown in Fig. 8A and B, the QC samples gathered closely in both PCA score plots, indicating the stability of the UPLC-QTOF/MS system throughout the analysis. The CON, Yang$_{syn}$, and Yin$_{syn}$ groups can be well

**Table 1** Identified differential metabolites

| ESI | m/z | RT (min) | KEGG | Metabolite | (Yang$_{syn}$+BGZ) vs. (Yang$_{syn}$) | (Yin$_{syn}$+BGZ) vs. (Yin$_{syn}$) |
|-----|-----|----------|------|------------|----------------------------------------|--------------------------------------|
| − | 145.0132 | 0.9378 | C00026 | α-Ketoglutarate | ↑* | ↓ |
| − | 455.0965 | 2.9226 | C00061 | Riboflavin-5-phosphate | ↑* | ↓* |
| − | 104.0348 | 0.8028 | C00065 | L-Serine | ↑ | ↓* |
| + | 113.0352 | 0.9136 | C00106 | Uracil | ↓* | ↑* |
| + | 778.5407 | 13.2262 | C00157 | Phosphatidylcholine | ↑ | ↓ |
| − | 582.5100 | 13.2602 | C00195 | N-Acylsphingosine | ↑** | ↓* |
| − | 148.0378 | 1.3859 | C00250 | Pyridoxal | ↑* | ↓* |
| − | 243.0615 | 1.3509 | C00299 | Uridine | ↓ | ↑* |
| − | 102.0556 | 0.8313 | C00334 | gamma-Aminobutyric acid | ↑* | ↓* |
| − | 766.6037 | 9.3765 | C00350 | Phosphatidylethanolamine | ↓** | ↑* |
| − | 240.0224 | 1.5073 | C00352 | Glucosamine 6-phosphate | ↑* | ↓** |
| − | 151.0569 | 0.9235 | C00379 | D-Xylitol | ↑ | ↓* |
| − | 671.4653 | 13.3460 | C00416 | Phosphatidate | ↓*** | ↑* |
| + | 173.0922 | 0.8994 | C00430 | 5-Aminolevulinate | ↓** | ↑ |
| + | 160.0756 | 1.9497 | C00483 | Tyramine | ↓* | ↑* |
| − | 583.2469 | 8.6720 | C00486 | Bilirubin | ↑ | ↓* |
| + | 583.2554 | 8.0917 | C00500 | Biliverdin | ↑** | ↓* |
| + | 90.0555 | 0.8565 | C00546 | Methylglyoxal | ↑ | ↓* |
| − | 397.2291 | 11.6884 | C00584 | Prostaglandin E2 | ↓** | ↑* |
| − | 229.0667 | 1.6209 | C00588 | Phosphorylcholine | ↑* | ↓* |
| + | 426.3162 | 15.2409 | C00695 | Cholic acid | ↑ | ↓** |
| + | 252.0724 | 2.1330 | C00818 | Glucaric acid | ↑ | ↓* |
| + | 465.3556 | 11.5639 | C01724 | Lanosterin | ↑ | ↓* |
| + | 799.6627 | 15.2528 | C01829 | Thyroxine | ↑** | ↓ |
| + | 196.0943 | 4.0050 | C03264 | D-Leucate | ↑** | ↓ |
| − | 187.1076 | 1.3080 | C02727 | N6-Acetyl-L-lysine | ↑* | ↓* |
| + | 560.3333 | 8.4013 | C03033 | beta-D-Glucuronoside | ↑* | ↓ |
| − | 205.0645 | 1.7274 | C03227 | 3-Hydroxy-L-kynurenine | ↓* | ↑* |
| + | 522.3564 | 9.5634 | C04230 | 1-Acyl-sn-glycero-3-phosphocholine | ↑** | ↓ |
| − | 401.0785 | 6.4160 | C04352 | (R)-4'-Phosphopantothenoyl-L-cysteine | ↑** | ↓*** |
| + | 381.0794 | 0.9636 | C04778 | N1-(5-Phospho-a-D-ribosyl)-5,6-dimethylbenzimidazole | ↓* | ↑** |
| − | 347.1835 | 8.9063 | C05302 | 2-Methoxyestradiol | ↑ | ↓** |
| − | 526.0585 | 1.3859 | C05381 | 3-Carboxy-1-hydroxypropylthiamine diphosphate | ↓ | ↑* |
| + | 389.2142 | 4.7813 | C05476 | Tetrahydrocorticosterone | ↑** | ↓ |
| − | 183.0346 | 0.8099 | C05580 | 3,4-Dihydroxymandelate | ↓ | ↑* |
| − | 297.0703 | 0.9593 | C05648 | 5-Hydroxy-N-formylkynurenine | ↑ | ↓* |
| − | 577.3444 | 13.7089 | C05789 | L-Urobilinogen | ↓* | ↑ |
| − | 365.2324 | 6.4089 | C14777 | 12(S)-HETE | ↓* | ↑* |
| + | 353.2472 | 6.4221 | C16513 | Docosapentaenoic acid (22n-3) | ↑* | ↓* |
| + | 136.0396 | 1.6256 | C22040 | Methylcysteine | ↑* | ↓** |

*P < 0.05, **P < 0.01, ***P < 0.001*

Zhang *et al. Chinese Medicine*    (2023) 18:102

Page 14 of 23

distinguished, suggesting that the metabolic information between the Yang$_{syn}$ and Yin$_{syn}$ groups has been changed. OPLS-DA analysis found that the comparison between the Yang$_{syn}$ group and the Yang$_{syn}$+BGZ groups (Fig. 8C and D) could both be significantly separated under ESI+ and ESI- modes, and the comparison between the Yin$_{syn}$ group and Yin$_{syn}$+BGZ group (Fig. 8E, F) could also be significantly separated under ESI+ and ESI- modes, and the permutation tests for OPLS-DA analysis revealed the models were not overfitted (Additional file 1: Fig. S2), indicating that significant metabolic disturbance occurred in the Yang$_{syn}$+BGZ group and Yin$_{syn}$+BGZ group after BGZ treatment. A total of 40 metabolites were identified based on *m/z* and corresponding secondary fragment ion characteristic maps (Table 1, Additional file 1: Fig. S3). Among the metabolites, 27 metabolites were markedly changed in the Yang$_{syn}$+GBZ group compared with the Yang$_{syn}$ group, and 31 metabolites were significantly changed in the Yin$_{syn}$+GBZ group compared with the Yin$_{syn}$ group. The heatmap for the above differential metabolites is presented in Fig. 8G.

## Correlation analysis of the relative abundance of metabolites and the levels of serum biochemistry (ALT and AST)

By analyzing the correlations between serum biochemistry (ALT and AST) and differential metabolites (Figs. 9), 20 metabolites, including 3 positive and 17 negative correlations, were significantly correlated with ALT, and 12 metabolites, including 3 positive and 9 negative correlations, were significantly correlated with AST.
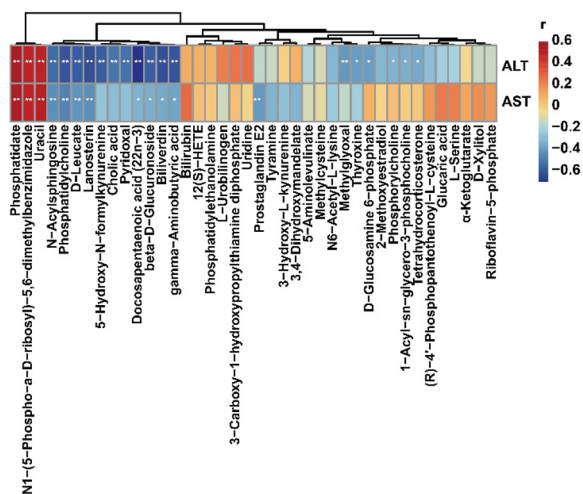


**Fig. 9** Heatmap of correlation between the levels of serum biochemistry (ALT and AST) and the relative abundance of metabolites (N = 6 ~ 8). The color depth represents correlation strength, the red color represents positive correlation, and the blue color represents negative correlation. *P < 0.05, **P < 0.01, ***P < 0.001

The correlation coefficient r and *P-value* are shown in Additional file 1: Table S6. Among them, Phosphatidate, Uracil, Prostaglandin E2, and N1-(5-Phospho-a-D-ribosyl)-5,6-dimethylbenzimidazole were all significantly positively correlated with ALT and AST, and Phosphatidylcholine, Lanosterin, N-Acylsphingosine, D-Leucate, Gamma-aminobutyric acid, Biliverdin, beta-D-Glucuronoside, and Docosapentaenoic acid (22n-3) were all significantly negatively correlated with ALT and AST.

## ROC curve analysis of metabolites

As shown in Additional file 1: Figs. S4, 9 metabolites had better discrimination between the Yang$_{syn}$+BGZ group and Yang$_{syn}$ group, and 5 metabolites had better discrimination between the Yin$_{syn}$+BGZ group and Yin$_{syn}$ group (all the areas under the curve (AUC) of the ROC curves ≥ 0.9 and *P < 0.05*). Venn analysis showed the ROC results of metabolites and their correlation with the levels of ALT and AST among the comparison of the Yang$_{syn}$+BGZ group and Yang$_{syn}$ group (Fig. 10A) and the comparison of the Yin$_{syn}$+BGZ group and the Yin$_{syn}$ group (Fig. 10B). Among them, Phosphatidate, Phosphatidylcholine, D-Leucate, and Biliverdin may be used as potential hepatoprotective biomarkers for the treatment of Yang$_{syn}$ (Fig. 10C–E), while N1-(5-Phospho-a-D-ribosyl)-5,6-dimethylbenzimidazole may be used as a potential hepatotoxicity biomarker for the treatment of Yin$_{syn}$ (Fig. 10G).

## Comparison of overall metabolic profiles

To further understand the metabolic disorder of susceptible syndromes, the KEGG identification code of differential metabolites was used for pathway analysis via MetaboAnalyst 5.0 (https://www.metaboanalyst.ca/). The schematic diagram of the disturbed metabolic pathways changed by the treatment of BGZ for Yang$_{syn}$ and Yin$_{syn}$ rats is presented in Fig. 11A and B. The redder the bubble color, the smaller the *P* value of the metabolic pathway. The details for the value of *P* are shown in Additional file 1: Tables S7 and S8. The results showed that the metabolites of BGZ regulating liver function in rats with Yang$_{syn}$ mainly involved glycerophospholipid metabolism, arachidonic acid metabolism, pantothenate and coenzyme A (CoA) biosynthesis. The metabolites of BGZ regulating liver function in rats with Yin$_{syn}$ mainly involve pantothenate and the CoA biosynthesis, glycerophospholipid metabolism. To compare the differences in metabolic profiles for BGZ treatment on Yin$_{syn}$ and Yang$_{syn}$ rats, a network map was constructed based on the identified metabolites and enriched metabolic pathways. As shown in Fig. 11C, metabolic pathways and metabolites interacted with each other to form a complex network.

Zhang *et al. Chinese Medicine*      (2023) 18:102

Page 15 of 23
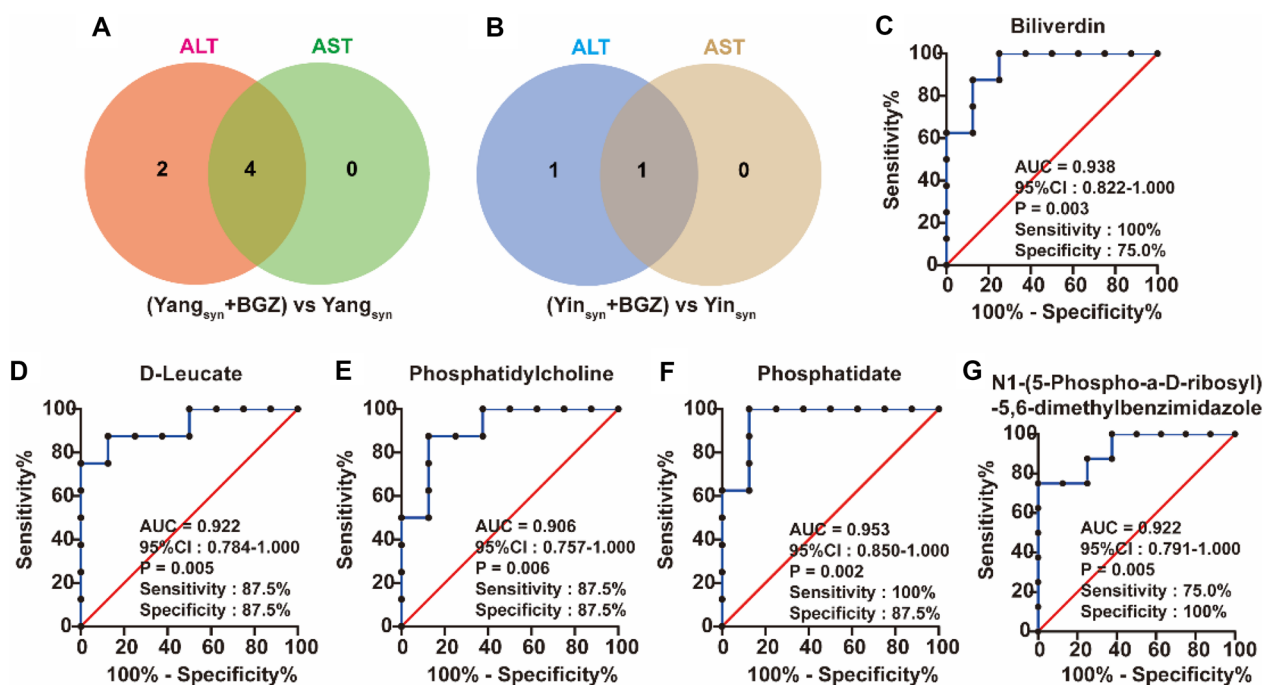


**Fig. 10** ROC analysis of metabolites associated with ALT and AST expression (N = 8). **A**–**B** Venn diagram showing the number of metabolites associated with the levels of ALT and AST under ROC ≥ 0.90 among the comparison of the $Yang_{syn}$+BGZ group and $Yang_{syn}$ group (**A**) and the comparison of the $Yin_{syn}$+BGZ group and the $Yin_{syn}$ group (**B**). **C**–**G** ROC curves of the above metabolites (Biliverdin (**C**), D-Leucate (**D**), Phosphatidylcholine (**E**), Phosphatidate (**F**), and ROC curves of N1-(5-Phospho-a-D-ribosyl)-5,6-dimethylbenzimidazole (**G**)) associated with the levels of ALT and AST under ROC ≥ 0.90.

## Integration analysis of "metabolites-genes-pathways" regulated by BGZ in rats with $Yin_{syn}$ and $Yang_{syn}$

In the Venn analysis of the metabolite enrichment pathways and DEGs enrichment pathways, it was found that the pathways of BGZ regulating liver function in rats with $Yin_{syn}$+BGZ were mainly involved in the glycine, serine and threonine metabolism, porphyrin and chlorophyll metabolism, arachidonic acid metabolism, amino sugar and nucleotide sugar metabolism, tryptophan metabolism (Fig. 12A), while the pathways regulated by BGZ in rats with $Yang_{syn}$+BGZ were mainly involved in the glycerolipid metabolism, tyrosine metabolism, riboflavin metabolism, beta-alanine metabolism (Fig. 12B). Figure 12 C and 12D visualized the network relationship among the "metabolites-genes-pathways" regulated by BGZ in rats with $Yin_{syn}$ and $Yang_{syn}$, respectively. It is worth noting that, the pathways of BGZ regulating in rats with $Yin_{syn}$ and $Yang_{syn}$ are almost all involved in energy metabolism, amino acid metabolism, lipid metabolism, and metabolism of cofactors and vitamins, and the above pathways were also cross-involved in $Na^+$-$K^+$-$ATP_{ase}$ and LDH [49, 50]. As shown in Fig. 12E F, the study further found the expression $Na^+$-$K^+$-$ATP_{ase}$ was significantly decreased in the $Yang_{syn}$ group ($P < 0.01$) but increased in the $Yin_{syn}$ group ($P < 0.01$) while compared with the CON

group. In addition, the levels of LDH were significantly increased in both model groups (both $P < 0.01$). Under BGZ intervention, the levels of $Na^+$-$K^+$-$ATP_{ase}$ in the $Yang_{syn}$+BGZ group and $Yin_{syn}$+BGZ group were both significantly increased when compared with corresponding model rats, respectively (both $P < 0.05$), while the levels of LDH in the $Yang_{syn}$+BGZ group and $Yin_{syn}$+BGZ group showed the opposite trends of change when compared with corresponding model rats, respectively (both $P < 0.05$).

## Discussion

Individual variability in liver injury following drug ingestion is a major challenge for DILI research and clinical prevention [1]. In the study, it was found that $Yin_{syn}$ and $Yang_{syn}$ are two different predisposed individual states of hepatotoxicity or hepatoprotection caused by BGZ. From the perspective of the gene expression profile, BGZ mostly does not affect normal rats, but it has a mild or greater impact on the change numbers of DEGs in $Yin_{syn}$ (28 DEGs) and $Yang_{syn}$ (102 DEGs) rats, respectively. From the perspective of endogenous metabolites, $Yin_{syn}$ and $Yang_{syn}$ rats can be well distinguished on the PCA scatter plot, and the OPLS-DA plot can further better distinguish $Yin_{syn}$, $Yang_{syn}$, and their corresponding
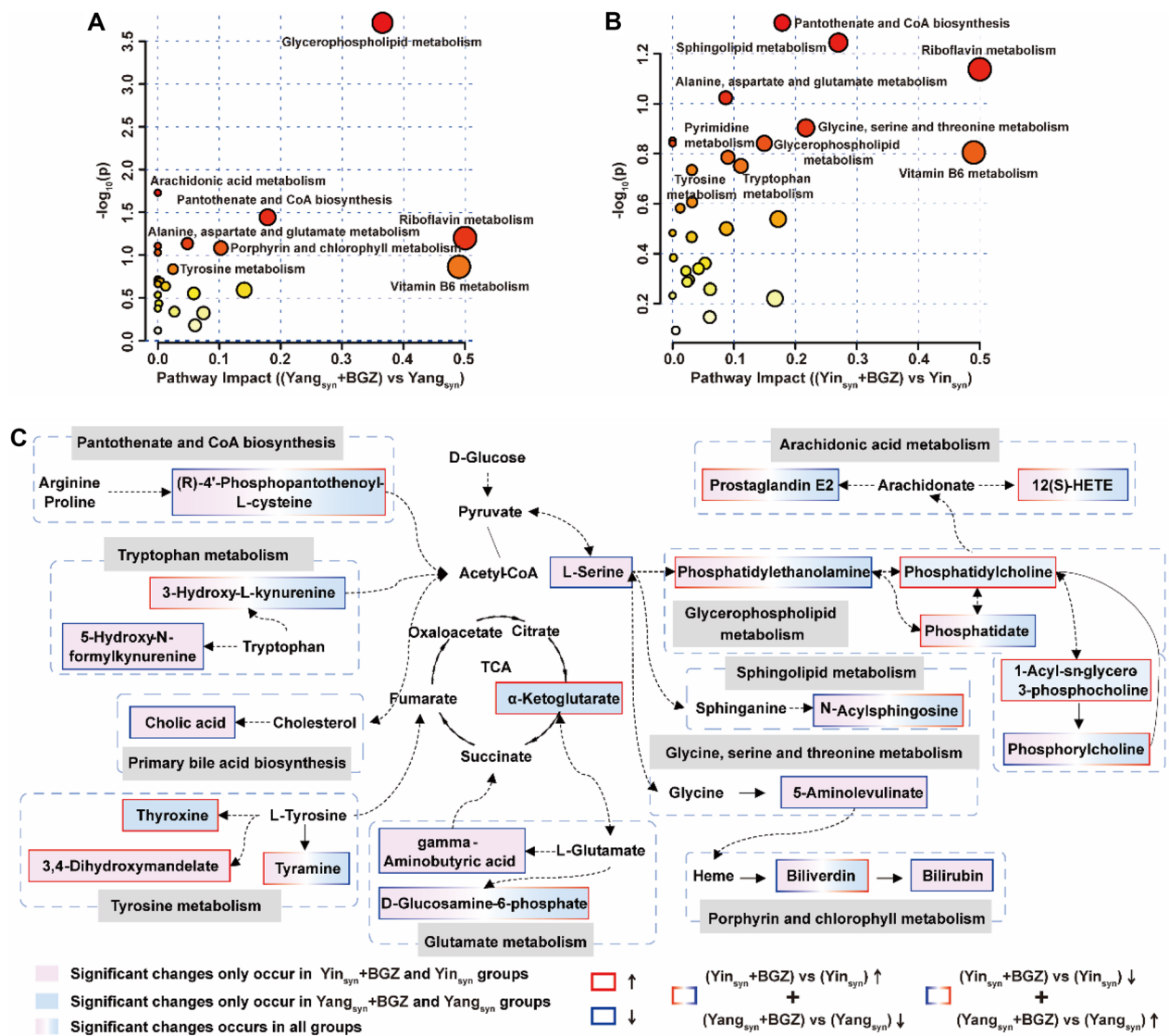
**Fig. 11** Overall metabolic profile. **A–B** Schematic diagram of the disturbed metabolic pathways for the BGZ treatment on Yang$_{syn}$ (**A**) and Yin$_{syn}$ (**B**) rats. **C** Correlation network diagram of DEGs and metabolism of BGZ intervention in Yin$_{syn}$ and Yang$_{syn}$ rats

BGZ-treated groups, suggesting that BGZ exerts different metabolic perturbation patterns for different models.

Among the DEGs with ROC ≥ 0.9 and significant correlation with ALT and AST, Slc25a25 may function as an ATP-Mg/Pi carrier to mediate the transport of Mg-ATP in exchange for phosphate. It is also likely responsible for the net uptake or efflux of adenine nucleotides into or from the mitochondria and is highly expressive in acute liver failure or induced by exogenous thyroxine [51, 52]. This study confirmed the high expression of Slc25a25 in the liver of Yin$_{syn}$ and Yang$_{syn}$ rats, which is consistent with the phenomenon of abnormal liver function [52]. However, only the expression of Slc25a25 in Yang$_{syn}$ rats

was inhibited by BGZ, indicating that Slc25a25 may be a hepatoprotective gene for BGZ in Yang$_{syn}$ rats, and the way to aggravate liver injury in rats with Yin$_{syn}$ may not by regulating Slc25a25. Pim3 is a liver growth-stimulating factor with serine/threonine kinase activity and is involved in gp130-mediated induction of cell proliferation and protection of apoptosis downstream of signal transducer and activator of transcription 3 (STAT3) [53, 54]. Pim3 is barely expressed in normal tissues but is highly expressed in the prostate, large intestine, liver, and other cancer tissues [55]. Therefore, its expression level is mainly used to evaluate tumor expression and metastasis [56, 57]. Pim3 is a kind of aldosterone regulatory protein

Zhang *et al. Chinese Medicine*    (2023) 18:102

Page 17 of 23
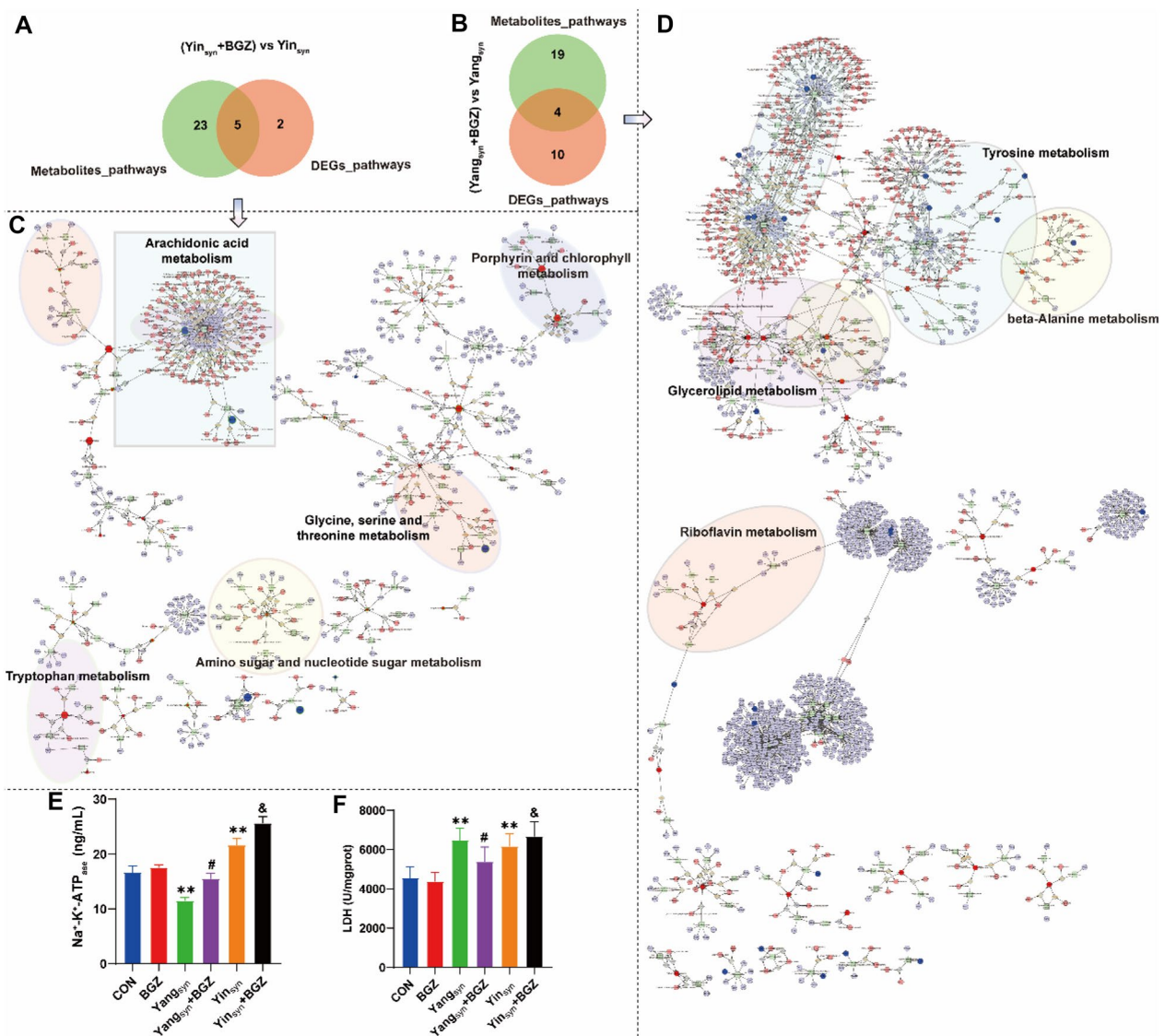
**Fig. 12** Integration analysis of "metabolites-genes-pathways" regulated by BGZ in rats with Yin_syn and Yang_syn. **A–B** Venn analysis of the crosstalk pathways of co-regulation of metabolites and DEGs by BGZ in Yin_syn (**A**) and Yang_syn (**B**) rats, **C–D** Visualization of the network relationship among the "metabolite-gene-pathway" regulated by BGZ in rats with Yin_syn (**C**) and Yang_syn (**D**). **E–F** Effect of BGZ treatment on the changes in the expression of Na$^+$-K$^+$-ATP_ase (**E**) and LDH (**F**) (N = 6 ~ 8). *$P < 0.05$, **$P < 0.01$, compared with CON group; #$P < 0.05$, compared with Yang_syn group; &$P < 0.05$, compared with Yin_syn group

with the ability to promote the expression of aldosterone [58], and the abnormal increase of aldosterone can increase the blood pressure of patients [59], which can result in the occurrence of heart, liver, and kidney damage in severe cases [60]. This study also found that the expression of Pim3 was positively correlated with the expression of ALT, which also suggested that the high expression of Pim3 may be another potential target for liver injury. Surprisingly, BGZ only decreased the expression of Pim3 in Yang_syn rats with almost no change in Yin_syn rats. The above results indicated that Pim3 may be

a marker gene for BGZ to exert a hepatoprotective effect on Yang_syn rats. In addition, BGZ may also have a potential therapeutic effect on tumor patients with Yang_syn, and the anti-tumor effect of BGZ has been confirmed [61, 62].

Among the metabolites with ROC ≥ 0.90 and significant correlation with ALT and AST, glycerophospholipids (including phosphatidylcholine, phosphatidylethanolamine, and phosphatidylserine) are the most abundant phospholipids in the body. In addition to constituting biofilm, they are also one of the components of bile and

Zhang *et al. Chinese Medicine*     (2023) 18:102

Page 18 of 23

membrane surface-active substances and participate in protein recognition and signal transduction through the cell membrane [63]. Hepatocytes can express various glycerophospholipids activities, making the liver an important organ for glycerophospholipid metabolism. Dysregulation of glycerophospholipids is related to the development and progression of liver diseases including hepatitis, liver cancer, fatty liver, and liver fibrosis [64]. For example, the abnormal change in the ratio of phosphatidylcholine to phosphatidylethanolamine will affect energy metabolism and is closely related to disease progression [65]. The changes in hepatic phospholipid composition are also associated with fatty liver disease and impaired postoperative liver regeneration [66–68].

In the glycerolipid metabolic pathway, phosphatidate can activate hepatic interleukin 6 (IL-6) signaling through inter-organ crosstalk and alleviate acetaminophen-induced liver injury in mice [68]. Phosphatidate also acts as an ionophore in the brain between depolarization and the release of neurotransmitters such as gamma-Aminobutyric Acid (GABA) [69]. The increase in the level of GABA can enhance the body's immunity under stress conditions [70] and has a good protective effect on acute liver injury or liver failure induced by ethanol, fluoride, and d-galactosamine [71–73]. In the study, under the intervention of BGZ, the expression of PE and GABA in the liver of rats with $Yin_{syn}$ and $Yang_{syn}$ both showed opposite trends, suggesting that regulating glycerophospholipid metabolism may be another way in which BGZ exerts liver damage and protection in $Yin_{syn}$ and $Yang_{syn}$ rats, respectively.

In the arachidonic acid metabolic pathway, 12(S)-HETE, as an important inflammatory marker, can affect the inflammatory process by stimulating the release of cytokines such as tumor necrosis factor alpha-like (TNF-α) and IL-6. Blocking the production of 12(S)-HETE can inhibit ischemia-reperfusion-induced liver dysfunction, inflammation, and cell death [74]. As a regulatory enzyme of arachidonic acid metabolism, arachidonate 15-lipoxygenase (Alox15) can catalyze it to 12(S)-HPETE, which is further reduced by glutathione peroxidase into 12(S)-HETE [75]. Prostaglandin E2 (PGE2), another metabolite of arachidonic acid, has also been shown to induce acute and chronic inflammation and various autoimmune diseases through Th1 differentiation, Th17 cell proliferation, and activation of mast cells [76]. Changes in arachidonic acid metabolism during liver ischemia can trigger the induction of inflammatory injury [77], arachidonic acid metabolism also plays an important role in galactosamine/endotoxin-induced acute liver injury in rats [78]. In this study, the relative expressions of 12(S)-HETE, PGE2, and Alox15 were significantly increased in the $Yin_{syn}$+BGZ group under the intervention of BGZ,

while the relative expressions of 12(S)-HETE and PGE2 were significantly decreased in the $Yang_{syn}$+BGZ group, suggesting that the regulation of arachidonic acid metabolism may be another way in which BGZ regulates the effects of liver protection or liver damage in rats with $Yang_{syn}$ and $Yin_{syn}$, respectively.

In the metabolic pathway of porphyrin and chlorophyll, porphyrins mediate related to tissue and cell damage by inducing protein oxidation and aggregation [79], and the liver is usually the source of excessive porphyrin production, porphyrin accumulation induced slight abnormalities of liver function and even liver failure is also a common type of tissue damage [80]. 5-aminolevulinate, the direct metabolite of glycine, can be used as a precursor of heme and participate in the regulation of the production of heme and its metabolite biliverdin [81]. Biliverdin has a good anti-inflammatory effect, can inhibit the expression of toll-like receptor 4 and nitric oxide, and reduces the inflammatory induction of lipopolysaccharide on macrophages [82]. It is used in the protection against various diseases (vascular injury, organ transplantation, etc.). As such, biliverdin can better reduce the ischemia-reperfusion injury in pig liver and have a liver protective effect [83]. Biliverdin reductase B (Blvrb) is a non-redundant nicotinamide adenine dinucleotide (phosphate)-dependent biliverdin reductase that regulates the cellular redox state by converting biliverdin to bilirubin. Its redox function also reduces intracellular reactive oxygen species accumulation [84] and maintains essential cytoprotective functions in recovery from hematopoietic stress [85]. Bilirubin is the main pigment in human bile and the main metabolite of iron porphyrin compounds in the body with certain damage to the brain and nerves [86]. The increase in its level can also lead to impaired liver function, so it is also used as a test for one of the common indicators of jaundice [87].

Blvrb has also been shown to catalyze the reduction of flavin mononucleotide (FMN, also known as Riboflavin-5-phosphate), flavin adenine dinucleotide (FAD), and riboflavin [88], and riboflavin is involved in tyrosine metabolism by sensitizing tyrosine photooxidation [89]. As an essential vitamin, riboflavin, especially its important derivatives FMN and FAD, disruption of riboflavin homeostasis were found to result in multiple systemic dysfunctions, including neuromuscular disease, anemia, fetal dysplasia, and cardiovascular disease [90]. For example, riboflavin (vitamin B2) deficiency can induce oxidative stress, which mediates the occurrence and development of liver injury and intestinal inflammation [91]. Riboflavin can also improve cardiac injury by inhibiting the expression of LDH induced by cardiac reoxygenation [92]. In addition, recent research demonstrates that tyrosine is abnormally elevated in patients with hepatitis,

Zhang *et al. Chinese Medicine*    (2023) 18:102

Page 19 of 23

biliary obstruction, or cirrhosis [93], and tyrosine kinase inhibitors can ameliorate liver injury induced by lipopolysaccharide and ischemia-reperfusion via inhibiting inflammation response [94, 95]. Small molecule multityrosine kinase inhibitors were also found could induced severe liver injury in the treatment of tumors [96]. In the study, BGZ significantly increased the expressions of biliverdin and FMN in Yang$_{syn}$ rats accompanied by the inhibition expressions of bilirubin and FMN in Yin$_{syn}$ rats, suggesting that the regulation of porphyrin and chlorophyll metabolism and tyrosine metabolism via Blvrb, may be a mechanism by which BGZ exerts hepatoprotective or liver damage effects on Yang$_{syn}$ and Yin$_{syn}$ rats, respectively.

In the metabolic pathway of tryptophan, tryptophan is involved in immune regulation, neural function, and intestinal homeostasis through the kynurenine pathway for metabolism [97]. For example, kynurenine is an endothelium-derived relaxation factor in the inflammatory process [98] and is metabolized to neurotoxic 3-Hydroxy-L-kynurenine under the action of kynureninase (Kynu), which is involved in the inflammatory process in psoriasis and other inflammatory diseases [99]. Tryptophan metabolism induces aromatic receptor activation and improves alcohol-induced liver injury [100], and supplementing tryptophan could also protect against CCl4-induced liver injury in rats by inhibiting LDH release [101]. Therefore, the imbalance of tryptophan metabolism in diseases ranging from cancer to neurodegenerative diseases has become a research hotspot for the therapeutic targeting of the kynurenine pathway [102]. In this study, compared with the Yang$_{syn}$ group and the Yin$_{syn}$ group, the levels of 3-Hydroxy-L-kynurenine were significantly decreased and increased under the intervention of BGZ, respectively, suggesting the kynurenine metabolism pathway in regulating tryptophan metabolism may be another mechanism by which BGZ exerts hepatoprotective or liver damage effects on Yang$_{syn}$ and Yin$_{syn}$ rats.

Glycine, serine and threonine metabolism are directly or indirectly involved in the above metabolic pathways (arachidonic acid metabolism, sphingolipid metabolism, porphyrin and chlorophyll metabolism) by providing raw materials [103–107]. Glycine, playing important roles in metabolic regulation, antioxidant response, and neurological function, has been widely used to prevent tissue damage, antioxidant and diabetes, obesity, ischemia-reperfusion injury, tumor, and other inflammatory diseases [108]. The decrease in serine level is closely related to the formation of fatty liver [109], and supplementing serine could alleviate alcoholic fatty liver by regulating homocysteine metabolism and adipogenesis [110]. Threonine can reduce chromium-induced oxidative stress and

inflammation by activating PI3K/AKT-related signaling pathways, thereby alleviating liver cell damage [111].

The above-discussed pathways changed by BGZ in Yin$_{syn}$ and (or) Yang$_{syn}$, were almost all related to energy metabolism, amino acid metabolism, and lipid metabolism, and the disorder of the above pathways has also been reported in Yin$_{syn}$ and Yang$_{syn}$ [112, 113]. The effects of BGZ on the metabolism of the above pathways have also been reported by Xu et al. [114]. cAMP, the potential biomarkers for Yin/Yang disharmony in TCM [115], can cross-activate protein kinases related to tissue biosynthesis and metabolism (including carbohydrates, lipids, amino acids, cofactors, and vitamins) as cyclic nucleotide effectors [116–118]. LDH and Na$^+$-K$^+$-ATP$_{ase}$, two indexes directly reflecting energy level, were significantly correlated with cAMP expression [119, 120]. Considering that BGZ can enhance the expression of cAMP-responsive element modulator-τ [121], and the opposite effect of BGZ on cAMP and LDH and the same adjustment trend on Na$^+$-K$^+$-ATP$_{ase}$, in rats with Yin$_{syn}$ and Yang$_{syn}$, respectively. It is suggested that the cAMP signaling pathway may be one of the mechanisms by which BGZ regulates energy metabolism to affect rats with Yin$_{syn}$ or Yang$_{syn}$. As for the different intervention effects of BGZ on the different syndromes, the interaction of endogenous metabolites and genes may be the main reason, which is worthy of further study in the future.

In conclusion, this study found that BGZ has a double-edged sword-like effect that not only exerts a good hepatoprotective effect on Yang$_{syn}$ rats but also has a potential risk of inducing liver injury in Yin$_{syn}$ rats. The mechanism is mainly reflected in BGZ having different regulatory effects on amino acid metabolism, energy metabolism, lipid metabolism, and metabolism of cofactors and vitamins in the above two different syndromes. In response to the seemingly contradictory results that BGZ has both liver-damaging and liver-protective effects in previous reports [6, 19], this study found that BGZ may have both liver-damaging and liver-protecting effects on predisposed individuals from the perspective of TCM syndrome theory. The study screened out the endogenous markers that can characterize the corresponding predisposed individuals, which will provide a certain reference for the safe and rational application of TCM.

## Supplementary Information

---

**Additional file 1: Table S1** Primer sequences of target genes. **Table S2** DEGs and correspondingfold changes (FC) regulated by BGZ in the treatment of Yang$_{syn}$ inrats. **Table S3** DEGs and correspondingfold changes regulated by BGZ in the treatment of Yin$_{syn}$ in rats. **Table S4**

---

Zhang *et al. Chinese Medicine*     (2023) 18:102

Page 20 of 23

The relationship between the relativeabundance ofDEGsand the levels of serum biochemistry (ALT and AST). **Table S5** GO functional enrichmentpathways analysis of DEGs regulated by BGZ in Yang$_{syn}$+BGZ ratscompared with Yang$_{syn}$ rats (Padjust < 0.05). **Table S6** The relationship between the relativeabundance of metabolites and the levels of serum biochemistry(ALT and AST). **Table S7** Metabolic pathways of BGZin the treatment of Yin$_{syn}$ in rats. **Table S8** Metabolic pathways of BGZin the treatment of Yang$_{syn}$ in rats. **Figure S1** ROC analysis of DEGs. **A** the DEGs between the Yang$_{syn}$+BGZ group and the Yang$_{syn}$group; **B** the DEGs between the Yin$_{syn}$+BGZ group and the Yin$_{syn}$group. **Figure S2 A** The 100-permutationtest for the Yang$_{syn}$+BGZ group and Yang$_{syn}$ group in ESI-mode; **B** The 100-permutation test for Yin$_{syn}$+BGZ group and Yin$_{syn}$group in ESI- mode; **C** The 100-permutation test for Yang$_{syn}$+BGZ groupand Yang$_{syn}$ group in ESI+ mode; **D** The 100-permutation test for Yin$_{syn}$+BGZgroup and Yin$_{syn}$ group in ESI+ mode. **Figure S3** Secondaryfragment ions characteristic maps of identified metabolites. **Figure S4** ROC analysis ofmetabolites. **A** the metabolites between the Yang$_{syn}$+BGZ group and theYang$_{syn}$ group; **B** the metabolites between the Yin$_{syn}$+BGZgroup and the Yin$_{syn}$ group.

## Author contributions

Jin-Fa Tang, Xiao-He Xiao, and Yan-Ling Zhao conceived and designed the experiments; Ming-Liang Zhang performed the experiments, analyzed the data, and wrote the manuscript; De-Xin Kong, Yuan Gao was responsible for helping with the collection of experimental samples; Yu-Long Chen, Hui Zhang, Xiao-Yan Wang help to detect the metabonomic changes of liver samples, Xu Zhao and Ming Niu helped with data analysis, Zhao-Fang Bai, Wei-Xia Li, and Yu-Ming Guo reviewed the paper. All authors have reviewed the manuscript and approved the final version of the manuscript. All authors have read, revised, and approved the final manuscript.

## Declarations

### Competing interests

The authors declare no competing financial interests.

### Author details

[1]Henan Province Engineering Laboratory for Clinical Evaluation Technology of Chinese Medicine, The First Affiliated Hospital of Henan University of Traditional Chinese Medicine, Zhengzhou, China. [2]Senior Department of Hepatology, The Fifth Medical Center of PLA General Hospital, Beijing, China. [3]Military Institute of Chinese Materia, the Fifth Medical Center of PLA General Hospital, Beijing, China. [4]Henan University of Traditional Chinese Medicine, Zhengzhou, China. [5]School of Traditional Chinese Medicine, Capital Medical University, Beijing, China. [6]College of Pharmacy, Chengdu University of Traditional Chinese Medicine, Chengdu, China. [7]Department of Pharmacy, The Fifth Medical Center of PLA General Hospital, Beijing, China.

## Reference

1. Andrade RJ, Chalasani N, Björnsson ES, Suzuki A, Kullak-Ublick GA, Watkins PB, et al. Drug-induced liver injury. Nat Rev Dis Primers. 2019;5(1):58.
2. Kullak-Ublick GA, Andrade RJ, Merz M, End P, Benesic A, Gerbes AL, et al. Drug-induced liver injury: recent advances in diagnosis and risk assessment. Gut. 2017;66(6):1154–64.
3. Shen T, Liu Y, Shang J, Xie Q, Li J, Yan M, et al. Incidence and etiology of Drug-Induced Liver Injury in Mainland China. Gastroenterology. 2019;156(8):2230–2241e11.
4. Hoofnagle JH, Björnsson ES. Drug-Induced Liver Injury - types and phenotypes. N Engl J Med. 2019;381(3):264–73.
5. Zhang L, Niu M, Wei AW, Tang JF, Tu C, Bai ZF, et al. Risk profiling using metabolomic characteristics for susceptible individuals of drug-induced liver injury caused by *Polygonum* multiflorum. Arch Toxicol. 2020;94(1):245–56.
6. Wang L, Wang Y, Wee A, Soon G, Gouw ASH, Yang R, et al. Clinico-pathological features of Bu Gu Zhi-induced liver injury, a long-term follow-up cohort study. Liver Int. 2020;40(3):571–80.
7. Chen M, Suzuki A, Borlak J, Andrade RJ, Lucena MI. Drug-induced liver injury: interactions between drug properties and host factors. J Hepatol. 2015;63(2):503–14.
8. Chen M, Borlak J, Tong W. High lipophilicity and high daily dose of oral medications are associated with significant risk for drug-induced liver injury. Hepatology. 2013;58(1):388–96.
9. Chen M, Borlak J, Tong W. A model to predict severity of drug-induced liver injury in humans. Hepatology. 2016;64(3):931–40.
10. Hoofnagle JH, Bonkovsky HL, Phillips EJ, Li YJ, Ahmad J, Barnhart H, et al. HLA-B*35:01 and Green Tea-Induced Liver Injury. Hepatology. 2021;73(6):2484–93.
11. Li C, Rao T, Chen X, Zou Z, Wei A, Tang J, et al. HLA-B*35:01 allele is a potential biomarker for predicting *Polygonum* multiflorum-Induced Liver Injury in humans. Hepatology. 2019;70(1):346–57.
12. Nakamura R, Arakawa N, Tanaka Y, Uchiyama N, Sekine A, Mashimo Y, et al. Significant association between HLA-B*35:01 and onset of drug-induced liver injury caused by kampo medicines in japanese patients. Hepatol Res. 2023; May;53(5):440–449
13. Petros Z, Kishikawa J, Makonnen E, Yimer G, Habtewold A, Aklillu E. HLA-B(*)57 allele is Associated with concomitant anti-tuberculosis and antiretroviral drugs Induced Liver toxicity in Ethiopians. Front Pharmacol. 2017;8:90.
14. Daly AK, Donaldson PT, Bhatnagar P, Shen Y, Pe'er I, Floratos A, et al. HLA-B*5701 genotype is a major determinant of drug-induced liver injury due to flucloxacillin. Nat Genet. 2009;41(7):816–9.
15. Pezzani MD, Resnati C, Di Cristo V, Riva A, Gervasoni C. Abacavir-induced liver toxicity. Braz J Infect Dis. 2016;20(5):502–4.
16. Monshi MM, Faulkner L, Gibson A, Jenkins RE, Farrell J, Earnshaw CJ, et al. Human leukocyte antigen (HLA)-B*57:01-restricted activation of drug-specific T cells provides the immunological basis for flucloxacillin-induced liver injury. Hepatology. 2013;57(2):727–39.
17. Xu CF, Johnson T, Wang X, Carpenter C, Graves AP, Warren L, et al. HLA-B*57:01 confers susceptibility to Pazopanib-Associated Liver Injury in patients with Cancer. Clin Cancer Res. 2016;22(6):1371–7.
18. Chinese Pharmacopoeia Commission. Pharmacopoeia of the People's Republic of China. Beijing: Chinese Medical Science and Technology Press; 2020.
19. Zhang X, Zhao W, Wang Y, Lu J, Chen X. The Chemical Constituents and Bioactivities of Psoralea corylifolia Linn.: a review. Am J Chin Med. 2016;44(1):35–60.
20. Gupta AK, Anderson TF. Psoralen photochemotherapy. J Am Acad Dermatol. 1987;17(5 Pt 1):703–34.
21. McNeely W, Goa KL. 5-Methoxypsoralen. A review of its effects in psoriasis and vitiligo. Drugs. 1998;56(4):667–90.
22. Liu YL, Ge FL, Zhu JX, Jing J, Wang JB, Zhang YM, et al. Re-evaluation of liver injury associated with Buguzhi Preparations based on passive monitoring data and hospital case. Zhongguo Zhong Yao Za Zhi. 2019;44(19):4272–6.
23. Li CY, Niu M, Liu YL, Tang JF, Chen W, Qian G, et al. Screening for susceptibility-related factors and biomarkers of Xianling Gubao Capsule-Induced Liver Injury. Front Pharmacol. 2020;11:810.
24. Deng PY, Cai HD, Cheng JH, Dao WB. Liver damage caused by Zhuanggu Joint Pill: a report of 30 cases. Chin J New Drugs, 1996. (03):212–4.
25. Nam SW, Baek JT, Lee DS, Kang SB, Ahn BM, Chung KW. A case of acute cholestatic hepatitis associated with the seeds of *Psoralea* corylifolia (boh-Gol-Zhee). Clin Toxicol 2005;43(6):589–91.

Zhang *et al. Chinese Medicine*    (2023) 18:102

Page 21 of 23

26. Li ZJ, Abulizi A, Zhao GL, Wang T, Zhou F, Jiang ZZ, et al. Bakuchiol contributes to the hepatotoxicity of *Psoralea* corylifolia in rats. Phytother Res. 2017;31(8):1265–72.

27. Zhang C, Zhao JQ, Sun JX, Li HJ. Psoralen and isopsoralen from *Psoraleae* Fructus aroused hepatotoxicity via induction of aryl hydrocarbon receptor-mediated CYP1A2 expression. J Ethnopharmacol. 2022;297:115577.

28. Ge FL, Niu M, Han ZX, Cao JL, Wang JB, Bai ZF, et al. Landscape of Hepatobiliary adverse drug reactions related to preparations containing *Psoraleae* Fructus and its application in pharmacovigilance. Chin J Integr Med. 2021;27(11):832–7.

29. Dermatology Branch of China Association of Chinese Medicine. Expert consensus on traditional chinese medicine treatment of psoriasis in Dermatology Branch. Chin J Dermato Venemol Integ Trad W Med. 2018;17(03):273–7.

30. Dermatology Branch of China Association of Chinese Medicine. Expert Consensus on Chinese Medicine Treatment of Vitiligo. Chin J Dermato Veneral Integ Trad W Med. 2017;16(02):191–2.

31. Ge JR, Wang HM, Zheng HX, Luo YW, Wang JB, Zhao YM, et al. Traditional Chinese Medicine Expert Consensus on the prevention and treatment of primary osteoporosis. Chin J Osteoporos. 2020;26(12):1717–25.

32. Su SB, Lu A, Li S, Jia W. Evidence-based ZHENG: a traditional Chinese medicine syndrome. Evid Based Complement Alternat Med. 2012;2012:246538.

33. Jiang M, Chen YR. Study on the relationship between syndrome of deficiency of spleen and kidney in chronic bronchitis and cAMP and cGMP in plasma. J Fujian Coll TCM, 1995. (01):16–7.

34. Ding JW, Xia TL, Wang XL. Plasma cyclic nucleotide level in patients with chronic renal insufficiency and its relationship with kidney deficiency. Gansu J TCM, 1996. (06):39–41.

35. Bi ZQ, Zou LJ, Kang ZQ, Wang ZG, Cheng JX, Yang W et al. Relationship between plasma prostaglandin, cyclic nucleotide content and kidney deficiency in traditional chinese medicine in chronic nephritis. Acta Acad Med Sin, 1981. (04):283–5.

36. Zhang Y, Xu SY, Liu MN, Jia TY, Qu WJ, Han T, et al. Comparative Studies on Chemical Contents and Effect in Kidney-Yang Deficiency Rats of Salt-Processed Product and Wine-Processed Product of Cuscutae Semen. Evid Based Complement Alternat Med. 2019;2019:2049497.

37. Wang P, Sun H, Lv H, Sun W, Yuan Y, Han Y, et al. Thyroxine and reserpine-induced changes in metabolic profiles of rat urine and the therapeutic effect of Liu Wei Di Huang Wan detected by UPLC-HDMS. J Pharm Biomed Anal. 2010;53(3):631–45.

38. Ren S, Shao Y, Zhao X, Hong CS, Wang F, Lu X, et al. Integration of Metabolomics and Transcriptomics reveals major metabolic pathways and potential biomarker involved in prostate Cancer. Mol Cell Proteomics. 2016;15(1):154–63.

39. Lu Y, Shao M, Xiang H, Zheng P, Wu T, Ji G. Integrative transcriptomics and metabolomics explore the mechanism of kaempferol on improving nonalcoholic steatohepatitis. Food Funct. 2020;11(11):10058–69.

40. Wang S, Bai M, Miao MS. Diagnostic index and analysis of an animal model of yin deficiency syndrome. Chin J Comp Med. 2021;31(01):132–7.

41. Tang WW, Zhang HY, Li Q, Li J, Yang GL. Modeling method and model evaluation of animal model of kidney yang deficiency syndrome. Modernization ofTraditional Chinese Medicine and Materia Materia-World Science and Technology, 2021(04):1317–24.

42. Kim D, Langmead B, Salzberg SL. HISAT: a fast spliced aligner with low memory requirements. Nat Methods. 2015;12(4):357–60.

43. Li B, Dewey CN. RSEM: accurate transcript quantification from RNA-Seq data with or without a reference genome. BMC Bioinformatics. 2011;12:323.

44. Love MI, Huber W, Anders S. Moderated estimation of fold change and dispersion for RNA-seq data with DESeq2. Genome Biol. 2014;15(12):550.

45. Xie C, Mao X, Huang J, Ding Y, Wu J, Dong S, et al. KOBAS 2.0: a web server for annotation and identification of enriched pathways and diseases. Nucleic Acids Res. 2011;39(Web Server issue):W316-22.

46. Ish-Shalom S, Lichter A. Analysis of fungal gene expression by Real Time quantitative PCR. Methods Mol Biol. 2010;638:103–14.

47. Su G, Morris JH, Demchak B, Bader GD. Biological network exploration with Cytoscape 3. Curr Protoc Bioinform. 2014;47:1–24 8.13.

48. Basu S, Duren W, Evans CR, Burant CF, Michailidis G, Karnovsky A. Sparse network modeling and metscape-based visualization methods for the analysis of large-scale metabolomics data. Bioinformatics. 2017;33(10):1545–53.

49. Skou JC, Esmann M. The Na,K-ATPase. J Bioenerg Biomembr. 1992;24(3):249–61.

50. Khan AA, Allemailem KS, Alhumaydhi FA, Gowder SJT, Rahmani AH. The biochemical and clinical perspectives of Lactate dehydrogenase: an enzyme of active metabolism. Endocr Metab Immune Disord Drug Targets. 2020;20(6):855–68.

51. Fujimoto N, Kitamura S, Uramaru N, Miyagawa S, Iguchi T. Identification of hepatic thyroid hormone-responsive genes in neonatal rats: potential targets for thyroid hormone-disrupting chemicals. Toxicol Lett. 2018;286:48–53.

52. Lee YM, Choi DH, Cheon MW, Kim JG, Kim JS, Shin MG, et al. Changes in Mitochondria-Related Gene Expression upon Acupuncture at LR3 in the D-Galactosamine-Induced Liver Damage Rat Model. Evid Based Complement Alternat Med. 2022;2022:3294273.

53. Liu J, Qu X, Shao L, Hu Y, Yu X, Lan P, et al. Pim-3 enhances melanoma cell migration and invasion by promoting STAT3 phosphorylation. Cancer Biol Ther. 2018;19(3):160–8.

54. Wang Y, Liu C, Hu L. Cholesterol regulates cell proliferation and apoptosis of colorectal cancer by modulating miR-33a-PIM3 pathway. Biochem Biophys Res Commun. 2019;511(3):685–92.

55. Brault L, Gasser C, Bracher F, Huber K, Knapp S, Schwaller J. PIM serine/threonine kinases in the pathogenesis and therapy of hematologic malignancies and solid cancers. Haematologica. 2010;95(6):1004–15.

56. Qu Y, Zhang C, Du E, Wang A, Yang Y, Guo J, et al. Pim-3 is a critical risk factor in development and prognosis of prostate Cancer. Med Sci Monit. 2016;22:4254–60.

57. Zhou Z, Zhang R, Wang R, Zhang Y, Xu L, Chen J, et al. Expression of Pim-3 in colorectal cancer and its relationship with prognosis. Tumour Biol. 2016;37(7):9151–6.

58. Spirli A, Cheval L, Debonneville A, Penton D, Ronzaud C, Maillard M, et al. The serine-threonine kinase PIM3 is an aldosterone-regulated protein in the distal nephron. Physiol Rep. 2019;7(15):e14177.

59. Whaley-Connell A, Johnson MS, Sowers JR. Aldosterone: role in the cardiometabolic syndrome and resistant hypertension. Prog Cardiovasc Dis. 2010;52(5):401–9.

60. Calvier L, Martinez-Martinez E, Miana M, Cachofeiro V, Rousseau E, Sádaba JR, et al. The impact of galectin-3 inhibition on aldosterone-induced cardiac and renal injuries. JACC Heart Fail. 2015;3(1):59–67.

61. Wu C, Sun Z, Ye Y, Han X, Song X, Liu S. Psoralen inhibits bone metastasis of breast cancer in mice. Fitoterapia. 2013;91:205–10.

62. Yu B, Wang AH, Zhou K, Chai LJ, Liu L. Molecular Pathway of Psoralidin-Induced apoptosis in HepG2 cell line. Chin J Integr Med. 2019;25(10):757–62.

63. Hishikawa D, Hashidate T, Shimizu T, Shindou H. Diversity and function of membrane glycerophospholipids generated by the remodeling pathway in mammalian cells. J Lipid Res. 2014;55(5):799–807.

64. van der Veen JN, Kennelly JP, Wan S, Vance JE, Vance DE, Jacobs RL. The critical role of phosphatidylcholine and phosphatidylethanolamine metabolism in health and disease. Biochim Biophys Acta Biomembr. 2017;1859(9 Pt B):1558–72.

65. Li Z, Agellon LB, Allen TM, Umeda M, Jewell L, Mason A, et al. The ratio of phosphatidylcholine to phosphatidylethanolamine influences membrane integrity and steatohepatitis. Cell Metab. 2006;3(5):321–31.

66. Ling J, Chaba T, Zhu LF, Jacobs RL, Vance DE. Hepatic ratio of phosphatidylcholine to phosphatidylethanolamine predicts survival after partial hepatectomy in mice. Hepatology. 2012;55(4):1094–102.

67. Sasabe N, Keyamura Y, Obama T, Inoue N, Masuko Y, Igarashi Y, et al. Time course-changes in phosphatidylcholine profile during oxidative modification of low-density lipoprotein. Lipids Health Dis. 2014;13:48.

68. Clemens MM, Kennon-McGill S, Vazquez JH, Stephens OW, Peterson EA, Johann DJ, et al. Exogenous phosphatidic acid reduces acetaminophen-induced liver injury in mice by activating hepatic interleukin-6 signaling through inter-organ crosstalk. Acta Pharm Sin B. 2021;11(12):3836–46.

69. Harris RA, Schmidt J, Hitzemann BA, Hitzemann RJ. Phosphatidate as a molecular link between depolarization and neurotransmitter release in the brain. Science. 1981;212(4500):1290–1.

Zhang *et al. Chinese Medicine*      (2023) 18:102

Page 22 of 23

70. Abdou AM, Higashiguchi S, Horie K, Kim M, Hatta H, Yokogoshi H. Relaxation and immunity enhancement effects of gamma-aminobutyric acid (GABA) administration in humans. BioFactors. 2006;26(3):201–8.

71. Yang H, Xing R, Liu S, Yu H, Li P. Rescuing fluoride-induced damages in liver with gamma aminobutyric acid. Biochem Biophys Res Commun. 2017;491(1):19–24.

72. Wang S, Sui S, Liu Z, Peng C, Liu J, Luo D, et al. Protective roles of hepatic gamma-aminobutyric acid signaling in acute ethanol exposure-induced liver injury. J Appl Toxicol. 2018;38(3):341–50.

73. Hata T, Rehman F, Hori T, Nguyen JH. GABA, γ-Aminobutyric acid, protects against severe Liver Injury. J Surg Res. 2019;236:172–83.

74. Zhang XJ, Cheng X, Yan ZZ, Fang J, Wang X, Wang W, et al. An ALOX12-12-HETE-GPR31 signaling axis is a key mediator of hepatic ischemia-reperfusion injury. Nat Med. 2018;24(1):73–83.

75. Spector AA, Gordon JA, Moore SA. Hydroxyeicosatetraenoic acids (HETEs). Prog Lipid Res. 1988;27(4):271–323.

76. Tsuge K, Inazumi T, Shimamoto A, Sugimoto Y. Molecular mechanisms underlying prostaglandin E2-exacerbated inflammation and immune diseases. Int Immunol. 2019;31(9):597–606.

77. Konishi T, Lentsch AB. Changes in arachidonic acid metabolism during liver ischemia triggers induction of inflammatory injury. Hepatology. 2018;68(4):1642–3.

78. Meng XJ, Wang JL. Arachidonic acid metabolism in galactosamine/endotoxin induced acute liver injury in rats. J Tongji Med Univ. 1994;14(3):169–72.

79. Maitra D, Bragazzi Cunha J, Elenbaas JS, Bonkovsky HL, Shavit JA, Omary MB. Porphyrin-Induced protein oxidation and aggregation as a mechanism of Porphyria-Associated Cell Injury. Cell Mol Gastroenterol Hepatol. 2019;8(4):535–48.

80. Saggi H, Maitra D, Jiang A, Zhang R, Wang P, Cornuet P, et al. Loss of hepatocyte β-catenin protects mice from experimental porphyria-associated liver injury. J Hepatol. 2019;70(1):108–17.

81. Sansaloni-Pastor S, Varesio E, Lange N. Modulation and proteomic changes on the heme pathway following treatment with 5-aminolevulinic acid. J Photochem Photobiol B. 2022;233:112484.

82. Wegiel B, Gallo D, Csizmadia E, Roger T, Kaczmarek E, Harris C, et al. Biliverdin inhibits toll-like receptor-4 (TLR4) expression through nitric oxide-dependent nuclear translocation of biliverdin reductase. Proc Natl Acad Sci U S A. 2011;108(46):18849–54.

83. Andria B, Bracco A, Attanasio C, Castaldo S, Cerrito MG, Cozzolino S, et al. Biliverdin protects against liver ischemia reperfusion injury in swine. PLoS ONE. 2013;8(7):e69972.

84. Wu S, Li Z, Gnatenko DV, Zhang B, Zhao L, Malone LE, et al. BLVRB redox mutation defines heme degradation in a metabolic pathway of enhanced thrombopoiesis in humans. Blood. 2016;128(5):699–709.

85. Nesbitt NM, Malone LE, Liu Z, Jares A, Gnatenko DV, Ma Y, et al. Divergent erythroid megakaryocyte fates in Blvrb-deficient mice establish non-overlapping cytoprotective functions during stress hematopoiesis. Free Radic Biol Med. 2021;164:164–74.

86. Watchko JF, Tiribelli C. Bilirubin-induced neurologic damage–mechanisms and management approaches. N Engl J Med. 2013;369(21):2021–30.

87. Fawaz R, Baumann U, Ekong U, Fischler B, Hadzic N, Mack CL, et al. Guideline for the evaluation of Cholestatic Jaundice in Infants: joint recommendations of the North American Society for Pediatric Gastroenterology, Hepatology, and Nutrition and the european Society for Pediatric Gastroenterology, Hepatology, and Nutrition. J Pediatr Gastroenterol Nutr. 2017;64(1):154–68.

88. Cunningham O, Gore MG, Mantle TJ. Initial-rate kinetics of the flavin reductase reaction catalysed by human biliverdin-IXbeta reductase (BVR-B). Biochem J. 2000;345(Pt 2):393–9.

89. Silva E, Godoy J. Riboflavin sensitized photooxidation of tyrosine. Int J Vitam Nutr Res. 1994;64(4):253–6.

90. Balasubramaniam S, Christodoulou J, Rahman S. Disorders of riboflavin metabolism. J Inherit Metab Dis. 2019;42(4):608–19.

91. Zhu YY, Thakur K, Feng JY, Zhang JG, Hu F, Cespedes-Acuña CL, et al. Riboflavin Bioenriched Soymilk alleviates oxidative stress mediated Liver Injury, intestinal inflammation, and gut microbiota modification in B(2) depletion-repletion mice. J Agric Food Chem. 2022;70(12):3818–31.

92. Mack CP, Hultquist DE, Shlafer M. Myocardial flavin reductase and riboflavin: a potential role in decreasing reoxygenation injury. Biochem Biophys Res Commun. 1995;212(1):35–40.

93. Levine RJ, Conn HO. Tyrosine metabolism in patients with liver disease. J Clin Invest. 1967;46(12):2012–20.

94. Gyurkovska V, Ivanovska N. Tyrosine kinase inhibitor tyrphostin AG490 reduces liver injury in LPS-induced shock. Eur J Pharmacol. 2015;751:118–26.

95. Palumbo T, Nakamura K, Lassman C, Kidani Y, Bensinger SJ, Busuttil R, et al. Bruton tyrosine kinase inhibition attenuates liver damage in a mouse warm ischemia and reperfusion model. Transplantation. 2017;101(2):322–31.

96. Studentova H, Volakova J, Spisarova M, Zemankova A, Aiglova K, Szotkowski T, et al. Severe tyrosine-kinase inhibitor induced liver injury in metastatic renal cell carcinoma patients: two case reports assessed for causality using the updated RUCAM and review of the literature. BMC Gastroenterol. 2022;22(1):49.

97. Cervenka I, Agudelo LZ, Ruas JL. Kynurenines: Tryptophan's metabolites in exercise, inflammation, and mental health. Science. 2017;357(6349):eaaf9794.

98. Wang Y, Liu H, McKenzie G, Witting PK, Stasch JP, Hahn M, et al. Kynurenine is an endothelium-derived relaxing factor produced during inflammation. Nat Med. 2010;16(3):279–85.

99. Harden JL, Lewis SM, Lish SR, Suárez-Fariñas M, Gareau D, Lentini T, et al. The tryptophan metabolism enzyme L-kynureninase is a novel inflammatory factor in psoriasis and other inflammatory diseases. J Allergy Clin Immunol. 2016;137(6):1830–40.

100. Wrzosek L, Ciocan D, Hugot C, Spatz M, Dupeux M, Houron C, et al. Microbiota tryptophan metabolism induces aryl hydrocarbon receptor activation and improves alcohol-induced liver injury. Gut. 2021;70(7):1299–308.

101. Wang D, Verney E, Sidransky H. Protective effect of tryptophan and cysteine against carbon tetrachloride-induced liver injury. Exp Mol Pathol. 1985;43(3):364–74.

102. Platten M, Nollen EAA, Röhrig UF, Fallarino F, Opitz CA. Tryptophan metabolism as a common therapeutic target in cancer, neurodegeneration and beyond. Nat Rev Drug Discov. 2019;18(5):379–401.

103. Cook HW, Thomas SE, Xu Z. Essential fatty acids and serine as plasmalogen precursors in relation to competing metabolic pathways. Biochem Cell Biol. 1991;69(7):475–84.

104. Pearlman RJ, Aubrey KR, Vandenberg RJ. Arachidonic acid and anandamide have opposite modulatory actions at the glycine transporter, GLYT1a. J Neurochem. 2003;84(3):592–601.

105. Muthusamy T, Cordes T, Handzlik MK, You L, Lim EW, Gengatharan J, et al. Serine restriction alters sphingolipid diversity to constrain tumour growth. Nature. 2020;586(7831):790–5.

106. Bonkovsky HL, Guo JT, Hou W, Li T, Narang T, Thapar M. Porphyrin and heme metabolism and the porphyrias. Compr Physiol. 2013;3(1):365–401.

107. Saino T, Watson EL. Inhibition of serine/threonine phosphatase enhances arachidonic acid-induced [Ca2+]i via protein kinase A. Am J Physiol Cell Physiol. 2009;296(1):C88–96.

108. Wang W, Wu Z, Dai Z, Yang Y, Wang J, Wu G. Glycine metabolism in animals and humans: implications for nutrition and health. Amino Acids. 2013;45(3):463–77.

109. Sim WC, Lee W, Sim H, Lee KY, Jung SH, Choi YJ, et al. Downregulation of PHGDH expression and hepatic serine level contribute to the development of fatty liver disease. Metabolism. 2020;102:154000.

110. Sim WC, Yin HQ, Choi HS, Choi YJ, Kwak HC, Kim SK, et al. L-serine supplementation attenuates alcoholic fatty liver by enhancing homocysteine metabolism in mice and rats. J Nutr. 2015;145(2):260–7.

111. Fang Z, Li Y, Wang J, Wang X, Huang L, Sun L, et al. Alleviative Effect of Threonine on cadmium-induced liver injury in mice. Biol Trace Elem Res; 2022.

112. Jiang N, Liu HF, Li SD, Zhou WX, Zhang YX, Zhang Q, et al. An integrated metabonomic and proteomic study on Kidney-Yin Deficiency Syndrome patients with diabetes mellitus in China. Acta Pharmacol Sin. 2015;36(6):689–98.

113. Chen R, Wang J, Zhan R, Zhang L, Wang X, Integrated Systems Pharmacology, Urinary metabonomics, and quantitative real-time PCR analysis to uncover targets and metabolic pathways of the You-Gui

Zhang *et al. Chinese Medicine*      (2023) 18:102

Page 23 of 23

Pill in treating Kidney-Yang Deficiency Syndrome. Int J Mol Sci. 2019;20(15):3683.

114. Xu Y, Zhao Y, Xie J, Sheng X, Li Y, Zhang Y. The evaluation of toxicity induced by *Psoraleae* Fructus in rats using untargeted metabonomic method based on UPLC-Q-TOF/MS. Evid Based Complement Alternat Med. 2017;2017:6207183.

115. Wang X, Du Y, Wu C, Xu M, Liu Y, Di X. UHPLC-MS/MS analysis of cAMP and cGMP in rat plasma as potential biomarkers of Yin-Yang disharmony in traditional chinese medicine. J Pharm Anal. 2021;11(4):458–64.

116. Jiang H, Shabb JB, Corbin JD. Cross-activation: overriding cAMP/cGMP selectivities of protein kinases in tissues. Biochem Cell Biol. 1992;70(12):1283–9.

117. Francis SH, Corbin JD. Cyclic nucleotide-dependent protein kinases: intracellular receptors for cAMP and cGMP action. Crit Rev Clin Lab Sci. 1999;36(4):275–328.

118. Coelho Horta B, Steinberg Perilo C, Caldeira Costa D, Nogueira-Machado JA. Martins Chaves, Aging: functional metabolic balance among cAMP, cGMP and reactive oxygen intermediate generation by human granulocytes. Gerontology. 2005;51(6):363–8.

119. Barguil Nepomuceno D, DÁvila Pessoa GC, Nascimento Araújo R, Barbosa Koerich L, Viana Sant'Anna MR, Horácio M, Pereira, et al. Na+/K+-ATPase activation by cAMP in the midgut of Lutzomyia longipalpis (Lutz & Neiva, 1912; *Diptera*: *Psychodidae*). J Insect Sci. 2022;22(2):1.

120. Li ZQ, Mårdh S. Interactions between Ca2+- and cAMP-dependent stimulatory pathways in parietal cells. Biochim Biophys Acta. 1996;1311(2):133–42.

121. Wei SM, Yan ZZ, Zhou J. Psoralea corylifolia protects against testicular torsion/detorsion-induced ischemia/reperfusion injury. J Ethnopharmacol. 2011;137(1):568–74.

## Publisher's Note

Springer Nature remains neutral with regard to jurisdictional claims in published maps and institutional affiliations.